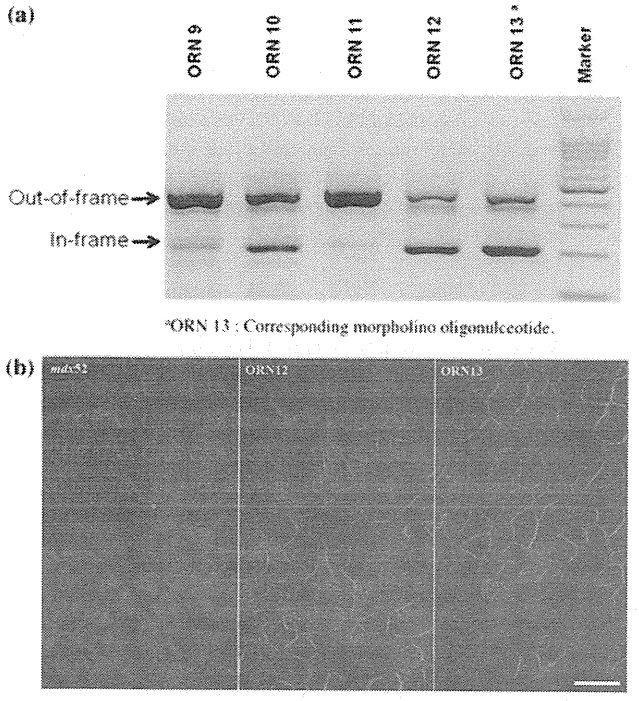

Figure 4. (a) One canonical example of the detection of antisence-mediated exon-skipping in *mdx*52 mice by reverse transcriptase polymerase chain reaction (RT-PCR). (b) Immunohistochemical staining of dystrophin in TA muscle of untreated and treated *mdx*52 mice (ORN 12 and ORN 13). There was no expression of dystrophin around the rim of any muscle fibers from untreated *mdx*52 mice. In contrast, restoration of dystrophin around the rim of muscle fibers was observed in both muscles from treated *mdx*52 by ORN12 and ORN 13. Dystrophin was detected with with dystrophin C-terminal antibody (*Dys-2*). Bar = 100 μm.

same as that of the corresponding morpholino nucleic acid (ORN 13, exon-skipping efficacy = 65%). We also evaluated the efficacy of ORN 12 by immunohistochemistry with dystrophin C-terminal antibody (*Dys-2*) as shown in part b. The number of dystrophin positive fibers was almost the same as that which resulted from ORN 13. These results indicated that the incorporation of 2′-*O*-MCE-Us into antisense RNA was effective for exon skipping.

■ CONCLUSIONS

In conclusion, we have developed an effective method for the synthesis of 2′-*O*-alkoxycarbonyl-ribonucleosides via Michael addition by using acrylate esters. We easily converted the MOCE group to the chemically stable MCE group by aminolysis. The amide group of the MCE group was not detrimental to the hybridization and enhanced metabolic stability. The phosphorothioate derivative of a 2′-*O*-Me-oligonucleotide incorporating six 2′-*O*-MCE-Us with a base sequence of mB30 proved to exhibit effective exon skipping in the splicing of the pre-mRNA of mouse dystrophin.

■ EXPERIMENTAL SECTION

Materials and Methods. All reagents and solvents obtained from commercial suppliers were used without further purification. All reactions were carried out under argon atmosphere in oven-dried glassware. NMR chemical shifts are given in parts per million (ppm); *J* values are given in hertz (Hz). ^{1}H and ^{13}C spectra were internally referenced to the appropriate residual undeuterated solvent. ^{31}P NMR was externally referenced with 85% H_3PO_4. Column chromatography was performed with silica gel C-200. Reversed phase HPLC on a C18 column was performed using a linear gradient of acetonitrile in 0.1 M ammonium acetate buffer. Anion-exchange HPLC was performed using a linear gradient of 0−100% solution A (20% CH_3CN in 0.5 M KH_2PO_4) in solution B (20% CH_3CN in 0.005 M KH_2PO_4). Thin-layer chromatography was performed using 60F-254 (0.25 mm). MALDI-TOF was measured in reflectron positive mode. The matrix condition was 3-hydroxypicolinic acid (HPA) 50 mg/mL in MeCN:H_2O (1:1, v/v), diammonium hydrogen citrate (AHC) 100 mg/mL in H_2O.

N^3-Benzoyl-2′-*O*-(2-methoxycarbonylethyl)-3′,5′-*O*-(1,1,3,3-tetraisopropyldisiloxane-1,3-diyl)uridine (6). To a solution of N^3-benzoyl-3′,5′-*O*-(1,1,3,3-tetraisopropyldisiloxane-1,3-diyl)uridine (5) (1.80 g, 3.03 mmol) in *t*-BuOH (15 mL) were added methyl acrylate (5.40 mL, 60.2 mmol) and cesium carbonate (489 mg, 1.39 mmol). The solution was stirred at ambient temperature for 4 h. The solution was extracted with EtOAc and saturated NH_4Cl. The organic layer was collected, dried over sodium sulfate, and concentrated under reduced pressure. The residue was chromatographed on silica gel. Elution with hexane/EtOAc (9:1, v/v) gave compound 6 (1.47 g, 2.17 mmol, 71%) as a white foam: ^{1}H NMR (500 MHz, DMSO-d_6) δ 8.00 (d, J = 8.0 Hz, 1H), 7.94−7.48 (m, 5H), 5.77 (d, J = 8.0 Hz, 1H), 5.75 (s, 1H), 4.27−4.04 (m, 6H), 4.00 (dd, J = 2.5, 13.5 Hz, 1H), 3.88 (d, J = 4.0 Hz, 1H), 3.62 (s, 3H), 2.60−2.58 (m, 2H), 1.11−0.97 (m, 28H); ^{13}C NMR (125 MHz, $CDCl_3$) δ 171.7, 168.9, 162.3, 149.1, 139.3, 135.4, 131.4, 130.7, 129.3, 101.6, 89.2, 82.6, 81.9, 68.2, 66.7, 59.5, 51.7, 35.2, 17.6, 17.4, 17.3, 17.1,17.0, 13.6, 13.2, 13.0, 12.6. HRMS m/z calcd for $C_{32}H_{49}N_2O_{10}Si_2$ $[M + H]^+$ 677.2926, found 677.2931.

N^3-Benzoyl-2′-*O*-(2-ethoxycarbonylethyl)-3′,5′-*O*-(1,1,3,3-tetraisopropyldisiloxane-1,3-diyl)uridine (7). To a solution of compound 5 (120 mg, 0.20 mmol) in *t*-BuOH (1 mL) were added cesium carbonate (65 mg, 0.20 mmol) and ethyl acrylate (0.43 mL, 4.0 mmol). The solution was vigorously stirred at ambient temperature for 18 h. The solution was extracted with EtOAc and saturated NH_4Cl aq. The organic layer was collected, dried over sodium sulfate, and concentrated under reduced pressure. The residue was chromatographed on silica gel. Elution with hexane/EtOAc (5:1, v/v) gave compound 7 (83 mg, 0.12 mmol, 60%): ^{1}H NMR (500 MHz, $CDCl_3$) δ 8.00 (d, J = 8.0 Hz, 1H), 7.93 (d, J = 7.5 Hz, 2H), 7.65 (dd, J = 7.5, 7.5 Hz, 1H), 7.50 (dd, J = 7.5, 7.5 Hz, 1H), 5.77 (d, J = 8.0 Hz, 1H), 5.75 (s, 1H), 4.09−3.88 (m, 9H), 2.65−2.55 (m, 2H), 1.09−0.85 (m, 31H). HRMS m/z calcd for $C_{33}H_{51}N_2O_{10}Si_2$ $[M + H]^+$ 691.3078, found 691.2997.

N^3-Benzoyl-2′-*O*-[2-[(2,2,2-trifluoroethoxy)carbonyl]ethyl]-3′,5′-*O*-(1,1,3,3-tetraisopropyldisiloxane-1,3-diyl)uridine (8). To a solution of compound 5 (9.00 g, 15.23 mmol) in *t*-BuOH (75 mL) were added 2,2,2-trifluoroethyl acrylate (30.2 g, 304.67 mmol) and cesium carbonate (4.96 g, 15.23 mmol). The solution was stirred at ambient temperature for 2 h. Then the solution was extracted with EtOAc and saturated NH_4Cl aq. The organic layer was collected, dried over sodium sulfate, and concentrated under reduced pressure. The residue was chromatographed on silica. Elution with hexane/EtOAc (6:1, v/v) gave compound 8 (8.29 g, 11.12 mmol, 73%): ^{1}H NMR (500 MHz, DMSO-d_6) δ 8.02 (d, J = 7.5 Hz, 2H), 7.85 (d, J = 8.0 Hz, 1H), 7.78 (dd, J = 7.0 Hz, 2H), 7.60 (dd, J = 7.5, 2 Hz), 5.82 (d, J = 8.0, 1 Hz), 5.64 (s, 1H), 4.66 (dd, J = 9.0, 13.0 Hz, 2H), 4.28−4.25 (m, 1H), 4.19−4.17 (m, 2H), 3.99−3.93 (m, 4H), 2.72 (dd, J = 6.0, 2 Hz), 1.05−0.94 (m, 27H); ^{13}C NMR (125 MHz, DMSO-d_6) δ 169.5, 169.4, 161.9, 148.6, 140.1, 135.5, 131.1, 130.3, 129.4, 100.6, 89.0, 81.2, 68.4, 65.9, 59.7, 59.5, 59.4, 34.3, 17.3, 17.2, 17.1, 17.0, 16.9, 16.84, 16.82, 16.7, 12.8, 12.3, 12.2, 11.9. HRMS m/z calcd for $C_{33}H_{48}F_3N_2O_{10}Si_2$ $[M + H]^+$ 745.2798, found 745.2781.

2′-*O*-(2-Methoxycarbonylethyl)-3′,5′-*O*-(1,1,3,3-tetraisopropyldisiloxane-1,3-diyl)uridine (9). To a solution of compound 6

(1.71 g, 2.53 mmol) in anhydrous THF (20 mL) was added *n*-$PrNH_2$ (1.5 mL, 18.0 mmol). The solution was vigorously stirred for 4 h. The solution was evaporated under reduced pressure. The residue was chromatographed on silica gel. Elution with hexane/EtOAc (1:4, v/v) gave compound **9** (1.03 g, 1.79 mmol, 71%) as a white foam: ^{1}H NMR (500 MHz, $CDCl_3$) δ 9.49 (s, 1H), 7.89 (d, J = 5.0 Hz, 1H), 5.73 (s, 1H), 5.67 (d, J = 5.0 Hz, 1H), 4.24−4.09 (m, 6H), 3.96−3.84 (m, 1H), 3.84 (s, 1H), 2.66−2.65 (m, 1H), 1.09−0.92 (m, 28H). HRMS m/z calcd for $C_{25}H_{45}N_2O_9Si_2$ $[M + H]^+$ 573.2663, found 573.2619.

2′-*O*-[2-(*N*-Methylcarbomoyl)ethyl]-3′,5′-*O*-(1,1,3,3-tetraisopropyldisiloxane-1,3-diyl)uridine (10). To a solution of compound **5** (1.80 g, 3.03 mmol) in *t*-BuOH (15 mL) were added cesium carbonate (489 mg, 1.39 mmol) and methyl acrylate (5.4 mL, 60.2 mmol). The solution was vigorously stirred at ambient temperature for 4 h. The suspension was diluted with EtOAc, and extracted with EtOAc and saturated $NaHCO_3$ aq. The organic layer was collected, dried over sodium sulfate, and concentrated under reduced pressure. The residue was treated with 40% $MeNH_2$ in MeOH (30 mL) at ambient temperature for 2 h. The solution was concentrated under reduced pressure. The residue was chromatographed on silica gel. Elution with hexane/EtOAc (1:1, v/v) gave compound **10** (1.14 g, 66%): ^{1}H NMR (500 MHz, $CDCl_3$) δ 9.90 (br, 1H), 7.91 (d, J = 8.0 Hz, 1H), 6.90 (br, 1H), 5.73−5.71 (m, 2H), 4.29−3.85 (7H, m), 2.81−2.79 (m, 3H), 2.63−2.47 (m, 2H). HRMS m/z calcd for $C_{25}H_{46}N_3O_8Si_2$ $[M + H]^+$ 572.2823, found 572.2826.

2′-*O*-[2-(*N*,*N*-Dimethylcarbamoyl)ethyl]3′,5′-*O*-(tetraisopropyldisiloxane-1,3-diyl)uridine (11). To a solution of compound **8** (240 mg, 0.32 mmol) in THF (3 mL) was added 2 M Me_2NH (2 mL). The solution was stirred for 2 h. The solution was concentrated under reduced pressure. The residue was chromatographed on silica gel. Elution with 5% MeOH in $CHCl_3$ gave compound **11** (152 mg, 0.26 mmol, 81%): ^{1}H NMR (500 MHz, $CDCl_3$) δ 9.56 (br, 1H), 7.85 (d, J = 5.0 Hz, 1H), 5.74 (s, 1H), 5.65 (d, J = 5.0 Hz, 1H), 4.19−4.06 (m, 5H), 3.92 (m, 1H), 3.85 (s, 1H), 3.03 (s, 3H), 2.91 (s, 3H), 1.01−0.90 (m, 28H). HRMS m/z $C_{26}H_{48}N_3O_8Si_2$ $[M + H]^+$ 586.2980, found 586.2921.

2′-*O*-[2-(*N*-Methylcarbomoyl)ethyl]uridine (13). A solution of compound **10** (563 mg, 0.98 mmol) in dry THF (10 mL) was treated with triethylamine trihydrofluoride (570 μL, 3.50 mmol) and triethylamine (253 μL, 1.80 mmol) at ambient temperature for 1 h. The solution was concentrated under reduced pressure. The residue was chromatographed on silica gel. Elution with 10% MeOH in $CHCl_3$ gave compound **13** (250 mg, 0.75 mmol, 76%): ^{1}H NMR (500 MHz, D_2O) δ 5.95 (d, J = 4.5 Hz, 1H), 5.92 (d, J = 8.5 Hz, 1H), 4.33 (t, J = 5.5 Hz, 1H), 4.17−4.12 (m, 2H), 3.98−3.88 (m, 3H), 3.79 (dd, J = 4.5, 13.0, 1H), 2.72−2.68 (m, 3H), 2.57−2.53 (m, 2H); ^{13}C NMR (125 MHz, D_2O) δ 175.0, 166.7, 152.0, 142.3, 102.9, 88.2, 85.1, 81.8, 68.9, 67.2, 61.1, 36.5, 26.4. HRMS m/z calcd for $C_{13}H_{20}N_3O_7$ $[M + H]^+$ 330.1301, found 330.1307.

5′-*O*-(4,4′-Dimethoxytrityl)-2′-*O*-[2-(methoxycarbonyl)ethyl]uridine (15). To a solution of compound **9** (780 mg, 1.37 mmol) in anhydrous THF (13 mL) was added $Et_3N \cdot 3HF$ (780 μL, 4.77 mmol). The solution was stirred at ambient temperature for 2 h. The solution was concentrated under reduced pressure. The residue was chromatographed on silica gel. Elution with 10% MeOH in $CHCl_3$ gave compound **12** as an intermediate, which was coevaporated three times with dry pyridine and finally dissolved in dry pyridine (13 mL). To the solution was added DMTrCl (510 mg, 1.50 mmol). The solution was stirred vigorously for 4 h. Then the solution was extracted with EtOAc and brine. The organic layer was collected, dried over sodium sulfate, and concentrated under reduced pressure. The residue was chromatographed on silica gel. Elution with EtOAc containing 0.5% Et_3N gave compound **15** (780 mg, 1.23 mmol, 90%): ^{1}H NMR (500 MHz, $CDCl_3$) δ 8.78 (br, 1H), 7.95 (d, J = 8.0 Hz, 1H), 7.28−7.21 (m, 9H), 6.82−6.80 (m, 4H), 5.91 (d, J = 1.5 Hz, 1H), 5.26 (d, J = 8.0 Hz, 1H), 4.49−4.45 (m, 1H), 4.04−3.92 (m, 4H), 3.76 (s, 6H), 3.68 (s, 3H), 3.50−3.45 (m, 3H), 2.70−2.56 (m, 2H). HRMS m/z calcd for $C_{34}H_{36}N_2NaO_{10}$ $[M + Na]^+$ 655.2268, found 655.2269.

(4,4′-Dimethoxytrityl)-2′-*O*-[2-(*N*-methylcarbamoyl)ethyl]-uridine (16). To a solution of compound **13** (553 mg, 1.67 mmol) in dry pyridine (15 mL) was added DMTrCl (622 mg, 1.84 mmol). The solution was stirred at ambient temperature for 4 h. The solution was diluted with EtOAc and washed with saturated $NaHCO_3$ aq. The organic layer was collected, dried over sodium sulfate, and concentrated under reduced pressure. The residue was chromatographed on silica gel. Elution with 2% MeOH in $CHCl_3$ containing 0.5% triethylamine gave compound **16** (740 mg, 1.17 mmol, 70%) as a white foam: ^{1}H NMR (500 MHz, $CDCl_3$) δ 7.95 (d, J = 8.0 Hz, 1H), 7.39−7.22 (9H, m), 6.86−6.83 (m, 4H), 5.93 (d, J = 3.0 Hz, 1H), 5.86 (br, 1H), 5.23 (d, J = 8.0 Hz, 1H), 3.97−3.90 (m, 2H), 3.79 (s, 3H), 3.54−3.48 (m, 2H), 2.81 (m, 3H), 2.61−2.43 (m, 2H); ^{13}C NMR (125 MHz, $CDCl_3$) δ 172.2, 163.6, 158.8, 150.8, 144.5, 140.3, 135.5, 135.3, 130.3, 130.2, 128.1, 127.3, 113.4, 102.4, 87.9, 87.2, 83.7, 82.9, 69.2, 66.6, 62.1, 55.4, 35.9, 26.5. HRMS m/z calcd for $C_{34}H_{37}N_3NaO_9$ $[M + Na]^+$ 654.2427, found 654.2446.

5′-*O*-(4,4′-Dimethoxytrityl)-2′-*O*-[2-(*N*,*N*-dimethylcarbamoyl)-ethyl]uridine (17). To a solution of compound **11** (3.61 g, 6.18 mmol) in THF (60 mL) was added $Et_3N \cdot 3HF$ (3.4 mL, 21.6 mmol). The solution was vigorously stirred for 4 h. The solution was evaporated under reduced pressure. The residue was chromatographed on silica gel. Elution with 10% MeOH in $CHCl_3$ gave compound **14** as an intermediate, which was coevaporated three times with anhydrous pyridine three times. The residue was dissolved in anhydrous pyridine (60 mL). To the solution was added DMTrCl (2.30 g, 6.80 mmol). The solution was vigorously stirred overnight. The solution was evaporated under reduced pressure. The residue was chromatographed on silica gel. Elution with 5% MeOH in $CHCl_3$ containing 0.5% Et_3N gave compound **17** (2.78 g, 4.32 mmol, 70%): ^{1}H NMR (500 MHz, $CDCl_3$) δ 8.72 (br, 1H), 7.92 (d, J = 8.0 Hz, 1H), 7.29−7.21 (m, 9H), 6.84−6.82 (m, 4H), 5.96 (d, J = 3.5 Hz, 1H), 5.36 (d, J = 3.5 Hz, 1H), 5.28 (d, J = 8.0 Hz, 1H), 4.59−4.56 (m, 1H), 4.11−4.07 (m, 2H), 4.00−3.98 (m, 1H), 3.90−3.87 (m, 1H), 3.79 (s, 6H), 3.54−3.44 (m, 2H), 3.00 (s, 3H), 2.96 (s, 3H), 2.78−2.75 (m, 1H), 2.45−2.41 (m, 1H). HRMS m/z calcd for $C_{35}H_{39}N_3NaO_9$ $[M + Na]^+$ 668.2584, found 668.2582.

Triethylamine Salt of 5′-*O*-(4,4′-Dimethoxytrityl)-2′-*O*-(2-carboxyethyl)uridine (18). To a solution of compound **15** (10 mg, 0.015 mmol) in pyridine (1 mL) was added 0.1 M NaOH (1 mL). The solution was stirred at ambient temperature for 30 min. The solution was extracted with $CHCl_3$ and 10% citric acid in H_2O. To the organic solution was added Et_3N (1 mL). The organic layer was dried over sodium sulfate and concentrated under reduced pressure to give compound **18** (7 mg, 0.0097 mmol, 65%): ^{1}H NMR ($CDCl_3$, 500 MHz) 8.08−7.16 (m, 14H), 6.83 (d, J = 10.0 Hz, 1H), 6.00 (d, J = 5.0 Hz, 1H), 5.31 (d, J = 10.0 Hz, 1H), 4.52−4.53 (m, 1H) 4.10−3.92 (m, 5H), 3.78 (s, 6H), 3.64−3.63 (m, 2H), 3.12−3.08 (m, 6H), 2.67−2.51 (m, 2H), 1.29−1.27 (m, 9H). HRMS m/z calcd for $C_{33}H_{34}N_2NaO_{10}$ $[M + Na]^+$ 641.2111, found 641.2174.

5′-*O*-(4,4′-Dimethoxytrityl)-2′-*O*-(2-carbamoylethyl)uridine-(19). To a solution of compound **15** (10 mg, 0.015 mmol) in pyridine (1 mL) was added 28% NH_4OH (1 mL). The solution was stirred at ambient temperature for 30 min. The solution was concentrated under reduced pressure to give compound **19** (10 mg, 0.015 mmol, 99%): ^{1}H NMR (CD_3CN, 500 MHz) δ 7.79 (d, J = 8.0 Hz, 1H), 7.53−7.34 (m, 11H), 6.98−6.96 (m, 11H), 6.50 (br, 1H), 5.99 (br, 1H), 5.89 (d, J = 4.0 Hz, 1H), 5.53 (s, 1H), 5.38 (d, J = 8.0 Hz, 1H), 4.48−4.46 (m, 1H), 4.08−4.05 (m, 2H), 3.92−3.86 (m, 2H), 3.50 (s, 6H), 3.41−3.39 (m, 2H), 2.60−2.51 (m, 2H); ^{13}C NMR (CD_3CN, 125 MHz) δ 174.9, 163.9, 159.7, 159.7, 151.4, 145.8, 141.1, 136.6, 136.4, 131.0, 131.0, 129.0, 128.9, 127.9, 118.3, 114.1, 114.1, 102.5, 88.3, 87.5, 84.2, 82.8, 70.0, 66.9, 63.4, 55.9, 35.7. HRMS m/z $C_{33}H_{35}N_3NaO_9$ $[M + Na]^+$ 640.2271, found 640.2257.

2′-*O*-[2-(Methoxycarbonyl)ethyl]-3′,5′-*O*-(1,1,3,3-tetraisopropyldisiloxane-1,3-diyl)adenosine (26). A solution of 3′,5′-*O*-(1,1,3,3-tetraisopropyldisiloxane-1,3-diyl)adenosine (**24**) (10.0 g, 19.6 mmol) in *t*-BuOH (100 mL) was treated with cesium carbonate (6.4 g, 19.6 mmol) at ambient temperature for 30 min. To the suspension was added methyl acrylate (35.5 mL, 392 mmol). The suspension was vigorously stirred for 9 h. The suspension was extracted with EtOAc and saturated NH_4Cl aq. The organic layer was collected, dried over sodium sulfate, and concentrated under reduced pressure. The residue was chromagraphed on silica gel. Elution with 0.5% MeOH in $CHCl_3$ gave compound **26** (8.40 g, 14.1 mmol, 72%): ^{1}H NMR (500 MHz, DMSO-d_6) δ 8.19 (s, 1H), 8.07 (s, 1H), 7.35−7.25 (br, 2H), 5.92 (s, 1H), 4.33 (dd, J = 4.0 Hz, 6.5 Hz, 1H), 4.47 (d, J = 4.0 Hz, 1H), 4.04−4.02 (m, 3H), 3.92−3.90 (m, 3H), 2.65−2.55 (m, 2H), 1.06 −0.95 (m, 28 H); ^{13}C NMR (125 MHz, $CDCl_3$) δ 171.3, 156.0, 152.5, 148.5, 139.2, 119.2, 87.5, 81.3, 80.6, 70.0, 66.5, 60.3, 51.2, 34.7, 17.2, 17.14, 17.10, 17.0, 16.9, 16.8, 16.7, 12.7, 12.3, 12.1, 12.1. HRMS m/z calcd for $C_{26}H_{45}N_5NaO_7Si_2$ $[M + Na]^+$ 618.2758, found 618.2772.

2′-*O*-[2-(Methoxycarbonyl)ethyl]-3′,5′-*O*-(1,1,3,3-tetraisopropyldisiloxane-1,3-diyl)cytidine (27). To the solution of 3′,5′-*O*-(1,1,3,3-tetraisopropyldisiloxane-1,3-diyl)cytidine (**25**) (5.0 g, 10.3 mmol) in *t*-BuOH (50 mL) was added cesium carbonate (3.33 g, 10.3 mmol). The suspension was stirred at ambient temperature for 30 min. To the suspension was added methyl acrylate (22.5 mL, 392 mmol). The suspension was vigorously stirred for 6 h. The suspension was extracted with EtOAc and saturated NH_4Cl aq. The organic layer was collected, dried over sodium sulfate, and concentrated under reduced pressure. The residue was chromatographed on silica gel. Elution with 2% MeOH in $CHCl_3$ gave compound **27** (4.41 g, 7.73 mmol, 75%): ^{1}H NMR (500 MHz, DMSO-d_6) δ 7.68 (d, J = 7.5 Hz, 1H), 7.19 (br, 1H), 5.68 (d, J = 7.5 Hz, 1H), 5.59 (s, 1H), 4.16−4.12 (m, 2H), 4.01−3.83 (m, 5H), 3.58 (s, 3H), 2.63−2.60 (t, J = 6.5 Hz, 2H), 1.06−0.92 (m, 28H); ^{13}C NMR (125 MHz, $CDCl_3$) δ 172.1, 166.3, 155.8, 140.8, 93.9, 89.4, 82.4, 81.4, 68.1, 66.5, 59.7, 51.7, 35.2, 17.6, 17.6, 17.4, 17.4, 17.2, 17.14, 17.11, 17.0, 13.5, 13.1, 13.0, 12.7. HRMS m/z calcd for $C_{25}H_{46}N_3O_8Si_2$ $[M + H]^+$ 572.2832, found 572.2738.

2′-*O*-[2-(Methoxycarbonyl)ethyl]-3′,5′-*O*-(1,1,3,3-tetraisopropyldisiloxane-1,3-diyl)-2-aminoadenosine (29). To a solution of 3′,5′-*O*-(1,1,3,3-tetraisopropyldisiloxane-1,3-diyl)-2-aminoadenosine (**28**) (11.0 g, 21.0 mmol) in *t*-BuOH (110 mL) were added cesium carbonate (7.03 g, 21.6 mmol) and methyl acrylate (39.1 mL, 431 mmol). The solution was stirred at ambient temperature for 18 h. The suspension was extracted with $CHCl_3$ and saturated NH_4Cl aq. The organic layer was collected, dried over sodium sulfate, and concentrated under reduced pressure. The residue was dissolved in $CHCl_3$ and absorbed with silica gel. The silica gel was subjected to a column. Elution with 3% MeOH in $CHCl_3$ gave compound **29** (10.1 g, 16.5 mmol, 79%): ^{1}H NMR (500 MHz, DMSO-d_6) δ 7.74 (s, 1H), 6.82−6.78 (br, 2H), 5.75 (s, 1H), 5.72 (s, 2H), 4.56 (dd, J = 5.0, 10 Hz, 1H), 4.30 (d, J = 5.0 Hz, 1H), 4.06−4.02 (m, 2H), 3.93−3.88 (m, 3H), 3.55 (s, 3H), 2.63−2,60 (m, 2H), 1.08−0,94 (m, 28H); ^{13}C NMR (125 MHz, DMSO-d_6) δ 171.3, 160.3, 156.1, 151.0, 134.5, 113.3, 86.3, 81.2, 80.5, 69.9, 66.3, 60.2, 51.3, 34.7, 17.3, 17.2, 17.1, 17.0, 16.9, 16.87, 16.80, 12,8, 12.4, 12.2, 12.1. HRMS m/z calcd for $C_{26}H_{47}N_6O_7Si_2$ $[M + H]^+$ 611.3039, found 611.3038.

6-*N*-Acetyl-2′-*O*-[2-(*N*-methylcarbamoyl)ethyl]adenosine (33). To a solution of compound **26** (4.70 g, 7.90 mmol) in EtOH (90 mL) was added 40% $MeNH_2$ in MeOH (90 mL). The solution was stirred at ambient temperature for 18 h. Then the solution was concentrated under reduced pressure. The residue was coevaporated three times with dry pyridine and finally dissolved in dry pyridine (90 mL). To the solution was added acetyl chloride (790 μL, 11.1 mmol). The solution was vigorously stirred for 6 h. The solution was diluted with EtOAc, and then extracted with EtOAc and saturated $NaHCO_3$ aq. The organic layer was collected, dried over sodium sulfate, and concentrated under reduced pressure to give compound **31** as an intermediate. The residue was coevaporated with toluene and dissolved in dry THF. To the solution were added triethylamine and triethylamine trihydrofluoride. The solution was vigorously stirred for 18 h. The solution was concentrated under reduced pressure. The residue was chromatographed on silica gel without aqueous workup. Elution with 3.5% MeOH in $CHCl_3$ gave compound **33** (1.87 g, 4.74 mmol, 60%): ^{1}H NMR (500 MHz, DMSO-d_6) δ 10.75−10.65 (br, 1H), 8.69 (s, 1H), 8.65 (s, 1H), 7.83 (d, J = 4.5 Hz, 1H), 6.06 (d, J = 6.0 Hz, 1H), 5.34 (d, J = 3.5 Hz, 1H), 5.18 (dd, J = 5.0 Hz), 4.57 (dd, J = 6.0 Hz, 1H), 4.41 (d, J = 3.0 Hz, 1H), 3.99 (d, J = 3.0 Hz, 1H), 3.08−3.76 (m, 1H), 3.69−3.33 (m, 3H), 2.51−2.52 (d, J = 4.5 Hz, 3H), 2.33−2.30 (m, 2H), 2.25 (s, 3H); ^{13}C NMR (125 MHz, DMSO-d_6) δ 170.8, 168.8, 151.7, 151.6, 149.6, 142.7, 123.7, 86.1, 85.6, 80.9, 68.9, 65.6, 61.2, 35.2, 25.4, 24.3. HRMS m/z calcd for $C_{16}H_{22}N_6NaO_6$ $[M + Na]^+$ 417.1499, found 417.1498.

4-*N*-Acetyl-2′-*O*-[2-(*N*-methylcarbamoyl)ethyl]cytidine (34). Compound **27** (2.90 g, 5.08 mmol) was treated with 40% $MeNH_2$ in MeOH (50 mL) at ambient temperature for 6 h. The solution was concentrated under reduced pressure and coevaporated three times with dry pyridine. The residue was dissolved with dry pyridine (50 mL), and to the solution was added acetyl chloride (398 μL, 5.58 mmol). The solution was vigorously stirred for 4 h. The solution was concentrated under reduced pressure, and coevaporated with toluene to give compound **32** as an intermediate. The residue was dissolved in THF, and to the solution were added TEA (1.25 mL, 8.63 mmol) and TEA·3HF (2.92 mL, 17.77 mmol). The solution was vigorously stirred for 18 h. The solution was concentrated under reduced pressure. The residue was chromatographed on silica gel. Elution with 7% MeOH in $CHCl_3$ gave compound **34** (994 mg, 2.68 mmol, 53%) as white foam: ^{1}H NMR (500 MHz, DMSO-d_6) δ 10.88 (s, 1H), 8.43 (d, J = 7.5 Hz, 1H), 7.84 (d, J = 4.0 Hz, 1H), 7.18 (d, J = 7.5 Hz, 1H), 5.80 (d, J = 2.5 Hz, 1H), 5.21 (dd, J = 5.0 Hz, 1H), 5.17 (d, J = 6.0 Hz, 1H), 4.08 (dd, J = 4.0, 6.0 Hz, 1H), 3.86−3.39 (m, 6H), 2.56 (d, J = 4.0 Hz, 1H), 2.39−2.35 (m, 2H), 2.09 (s, 3H). HRMS m/z calcd for $C_{15}H_{22}N_4O_7$ $[M + H]^+$ 371.1556, found 371.1516.

6-*N*-Acetyl-5′-*O*-(4,4′-dimethoxytrityl)-2′-*O*-[2-(*N*-methylcarbamoyl)ethyl]adenosine (35). To a solution of compound **33** (1.50 g, 3.80 mmol) in dry pyridine was added DMTrCl (1.05 g, 3.24 mmol). The solution was stirred at ambient temperature for 5 h. The solution was extracted with $CHCl_3$ and brine. The organic layer was collected, dried over sodium sulfate, and concentrated under reduced pressure. The residue was chromatographed on silica gel. Elution with 3% MeOH in $CHCl_3$ containing 0.5% Et_3N gave compound **35** (1.95 g, 2.80 mmol, 73%): ^{1}H NMR (500 MHz, DMSO-d_6) δ 10.70 (br, 1H), 8.57 (s, 1H), 8.56 (s, 1H), 7.83−7.82 (m, 1H), 7.33−7.17 (m, 9H), 6.84−6.80 (m, 4H), 6.09 (d, J = 5.0 Hz, 1H), 5.38 (d, J = 5.0 Hz, 1H), 4.71−4.69 (m, 1H), 4.49−4.47 (m, 1H), 4.09−4.08 (m, 1H), 3.82−3.67 (m, 8H), 3.21−3.16 (m, 2H), 2.50 (s, 3H), 2.33−2.25 (m, 2H), 2.11 (s, 3H). HRMS m/z calcd for $C_{37}H_{41}N_6O_8$ $[M + H]^+$ 697.2986, found 697.2946.

4-*N*-Acetyl-5′-*O*-(4,4′-dimethoxytrityl)-2′-*O*-[2-(*N*-methylcarbamoyl)ethyl]cytidine (36). To a solution of compound **34** (374 mg, 1.00 mmol) in dry pyridine (6 mL) was added DMTrCl (244 mg, 0.72 mmol). The solution was stirred at ambient temperature for 5 h. The solution was extracted with $CHCl_3$ and brine. The organic layer was collected, dried over sodium sulfate, and concentrated under reduced pressure. The residue was chromatographed on silica gel. Elution with 6% MeOH in $CHCl_3$ containing 0.5% Et_3N gave compound **36** (350 mg, 0.52 mmol, 52%): ^{1}H NMR (500 MHz, $CDCl_3$) δ 9.49 (br, 1H), 8.48 (d, J = 7.5 Hz, 1H), 7.41−7.23 (m, 9H), 6.85−6.83 (m, 4H), 6.52 (br, 1H), 5.89 (s, 1H), 4.49−4.45 (m, 2H), 4.15−3.92 (m, 4H), 3.79 (s, 3H), 3.79 (s, 3H), 3.54−3.54 (m, 2H), 2.76 (d, 3H),

dx.doi.org/10.1021/jo101963z |J. Org. Chem. 2011, 76, 3042–3053

2.62−2.39 (m, 2H), 2.18 (s, 3H). HRMS m/z calcd for $C_{36}H_{40}N_4NaO_9$ $[M + Na]^+$ 695.2693, found 695.2694.

5′-*O*-(4,4′-Dimethoxytrityl)-2′-*O*-[2-(*N*-methylcarbamoyl)-ethyl]uridine-3-(2-cyanoethyl-*N*,*N*-diisopropylphosphoramidite) (20). To a solution of compound **16** (490 mg, 0.77 mmol) in dry MeCN (2 mL) were added diisopropylammonium 1*H*-tetrazolide (101 mg, 1.19 mmol) and 2-cyanoethyl-*N*,*N*,*N*′,*N*′-tetraisopropylphosphordiamidite (358 mg, 1.19 mmol). The solution was stirred under argon atmosphere at ambient temperature for 8 h. The solution was diluted with EtOAc and washed with saturated $NaHCO_3$ aq. The organic layer was collected, dried over sodium sulfate, and concentrated under reduced pressure. The residue was chromatographed on silica gel. Elution with 1% MeOH in $CHCl_3$ containing 0.5% triethylamine gave compound **20** (384 mg, 0.46 mmol, 60%) as a white foam: ^{1}H NMR (500 MHz, $CDCl_3$) δ 8.09−8.01 (m, 1H), 7.47−7.27 (m, 9H), 6.86−6.82 (m, 4H), 6.49 (br, 1H), 5.90 (m, 1H), 5.28−5.21 (m, 1H), 4.61−4.48 (m, 1H), 4.25−3.86 (m, 4H), 3.80 −3.79 (m, 1H), 3.75−3.43 (m, 6H), 2.80−2.77 (m, 3H), 2.64−2.42 (m, 4H), 1.29−1.03 (m, 12H); ^{31}P NMR (125 MHz, $CDCl_3$) δ 151.32, 150.48. HRMS m/z calcd for $C_{43}H_{55}N_5O_{10}P$ $[M + H]^+$ 832.3687, found 832.3650.

6-*N*-Acetyl-5′-*O*-(4,4′-dimethoxytrityl)-2′-*O*-[2-(*N*-methylcarbamoyl)ethyl]adenosine-3′-(2-cyanoethyl-*N*,*N*-diisopropylphosphoramidite) (21). To a solution of compound **35** (1.00 g, 1.44 mmol) in dry MeCN (150 mL) were added 2-cyanoethyl-*N*,*N*,*N*′,*N*′-tetraisopropylphosphordiamidite (920 μL, 2.87 mmol) and diisopropylammonium 1*H*-tetrazolide (147 mg, 0.86 mmol) at ambient temperature for 18 h. The solution was concentrated under reduced pressure. The residue was chromatographed on silica gel. Elution with 3% MeOH in $CHCl_3$ gave compound **21** (980 mg, 1.09 mmol, 76%): ^{1}H NMR (500 MHz, $CDCl_3$) δ 8.63−8.61 (m, 2H), 8.26−8.22 (m, 1H), 7.42−7.21 (m, 9H), 6.82−6.79 (m, 4H), 6.41−6.38 (m, 1H), 6.16−6.15 (m, 1H), 4.69−4.59 (m, 2H), 4.40−4.33 (m, 1H), 4.04−3.97 (m, 1H), 3.90−3.85 (m, 2H), 3.79−3.62 (m, 6H), 3.60−3.52 (s, 4H), 3.39−3.35 (m, 1H); ^{31}P NMR (125 MHz, $CDCl_3$) δ 151.34, 151.30. HRMS m/z calcd for $C_{46}H_{58}N_8O_9P$ $[M + H]^+$ 897.4064, found 897.4022.

4-*N*-Acetyl-5′-*O*-(4,4′-dimethoxytrityl)-2′-*O*-[2-(*N*-methylcarbamoyl)ethyl]cytidine-3′-(2-cyanoethyl-*N*,*N*-diisopropylphosphoramidite) (22). To a solution of compound **36** (480 mg, 0.71 mmol) in dry MeCN (2 mL) were added diisopropylammonium 1*H*-tetrazolide (92 mg, 0.54 mmol) and 2-cyanoethyl-*N*,*N*,*N*′,*N*′-tetraisopropylphosphorodiamidite (343 μL, 1.07 mmol). The solution was stirred at ambient temperature for 10 h. The solution was extracted with $CHCl_3$ and brine. The organic layer was dried, collected over sodium sulfate, and concentrated under reduced pressure. The residue was chromatographed on silica gel. Elution with 1.5% MeOH in $CHCl_3$ containing 0.5% Et_3N gave compound **22** (300 mg, 0.34 mmol, 48%): ^{1}H NMR (500 MHz, $CDCl_3$) δ 9.70−9.67 (m, 1H), 8.63−8.56 (m, 1H), 7.34−6.86 (m. 11H), 5.93 (s, 1H), 4.57−4.48 (m, 1H), 4.30−4.02 (m 4H), 3.84−3.83 (m, 6H), 3.73−3.46 (m, 6H), 2.81−2.62 (m, 4H), 2.43−2.37 (m, 2H), 2.26 (s, 3H), 1.27−1.03 (m, 12H); ^{31}P NMR (125 MHz, $CDCl_3$) δ 151.43, 150.23. HRMS m/z calcd for $C_{45}H_{58}N_6O_{10}P$ $[M + H]^+$ 873.3952, found 872.3911.

2′-*O*-[2-(*N*-Methylcarbamoyl)ethyl]-3′,5′-*O*-(1,1,3,3-tetraisopropyldisiloxane-1,3-diyl)-2-aminoadenosine (37). To a solution of compound **29** (1.0 g, 1.64 mmol) in EtOH (8 mL) was added 40% methylamine in MeOH (8 mL) at ambient temperature for 18 h. The solution was concentrated under reduced pressure. The residue was chromatographed on silica gel. Elution with 4% MeOH in $CHCl_3$ gave compound **37** (770 mg, 1.26 mmol, 77%): ^{1}H NMR (500 MHz, DMSO-d_6) δ 7.76−7.74 (m, 2H), 6.82−6.76 (br, 2H), 5.75 (s, 1H), 5.73 (s, 2H), 4.54 (dd, J = 5.0, 8.0 Hz, 1H), 4.27 (d, J = 5.0 Hz, 1H), 4.06−3.98 (m, 2H), 3.94−3.90 (m, 2H), 3.87−3.82 (m, 1H), 2.53 (d, J = 4.0 Hz, 3H), 2.37 (dd, J = 6 Hz, 2H), 1.04−1.02 (m, 28H). HRMS m/z calcd for $C_{26}H_{48}N_7O_6Si_2$ $[M + H]^+$ 610.3198, found 610.3183.

2′-*O*-[2-(*N*-Methylcarbamoyl)ethyl]-2-*N*-phenoxyacetyl-3′,5′-*O*-(1,1,3,3-tetraisopropyldisiloxane-1,3-diyl)-2-aminoadenosine (38). To a solution of compound **37** (500 mg, 0.82 mmol) in dry pyridine (20 mL) at −10 °C was dropwise added phenoxyacetyl chloride (124 μL, 0.90 mmol) over 5 min. The solution was vigorously stirred at −10 °C for 2 h and then at ambient temperature for 1 h. The solution was diluted with $CHCl_3$ and extracted with brine. The organic layer was collected, dried over sodium sulfate, and concentrated under reduced pressure. Elution with 5% MeOH in $CHCl_3$ gave compound **38** (442 mg, 0.60 mmol, 73%): ^{1}H NMR (500 MHz, DMSO-d_6) δ 10.00 (s, 1H), 8.04 (s, 1H), 7.68 (d, J = 4.0 Hz, 1H), 7.50−7.38 (br, 2H), 7.29−7.26 (m, 2H), 6.37−6.91 (m, 3H), 5.88 (s, 1H), 5.02 (s, 2H), 4.53 (dd, J = 5.0, 8 Hz, 1H), 4.38 (d, J = 8.0 Hz, 1H), 4.11−4.08 (m, 1H), 4.03−3.86 (m, 4H), 2.49 (m, 3H), 2.33 (dd, J = 7.0, 7.0 Hz, 2H), 1.04−0.93 (m, 28H); ^{13}C NMR (125 MHz, DMSO-d_6) δ 170.1, 158.0, 156.1, 152.5, 149.4, 137.2, 129.4, 120.8, 116.1, 114.5, 86.8, 81.0, 80.9, 69.7, 67.4, 67.1, 60.4, 40.0, 36.1, 25.3, 17.3, 17.16, 17.12, 17.0, 16.9 16.8, 12.7, 12.3, 12,1, 12.0. HRMS m/z calcd for $C_{34}H_{53}N_7NaO_8Si_2$ $[M + Na]^+$ 766.3392, found 766.3400.

2′-*O*-[2-(*N*-Methylcarbamoyl)ethyl]-2-*N*-phenoxyacetylguanosine (30). To a stirred solution of compound **38** (1.00 g, 1.34 mmol) in AcOH (100 mL) were added H_2O (40 mL) and $NaNO_2$ (752 mg, 10.75 mmol). After 30 min another portion of $NaNO_2$ (752 mg, 10.75 mmol) was added. The solution was stirred at ambient temperature for 48 h. The solution was concentrated under reduced pressure to give a yellow syrup. The syrup was extracted once with brine and three times with saturated $NaHCO_3$ aq. The organic layer was dried, collected over sodium sulfate, and concentrated under reduced pressure to give compound **39** as an intermediate. The residue was coevaporated with dry pyridine. The residue was dissolved in anhydrous THF (130 mL). To the solution were added triethylamine (340 μL) and triethylamine trihydrofluoride (650 μL). The solution was stirred vigorously at ambient temperature for 6 h. The solution was concentrated under reduced pressure. The residue was extracted with H_2O and $CHCl_3$. After several minutes, white precipitates appeared in the aqueous layer. The aqueous layer was concentrated to reduce its volume. The precipitate was collected by filtrtion and dried. Finally, it was dried by vacuum and gentle heating to give compound **30** (490 mg, 0.97 mmol, 71%): ^{1}H NMR (500 MHz, DMSO-d_6) δ 11.84 (s, 1H), 11.78 (s, 1H), 8.29 (s, 1H), 7.89 (d, J = 4.0 Hz, 1H), 7.32−7.29 (m, 2H), 6.99−6.97 (m, 3H), 5.87 (d, J = 6.5 Hz, 1H), 5.30 (d, J = 3.5 Hz, 1H, diminished with D_2O), 5.09 (dd, J = 5.5, 5.5 Hz, 1H, diminished with D_2O), 4.86 (s, 2H), 4.44−4.42 (m, 1H), 4.38−4.37 (m, 1H), 3.95 (d, J = 2.0 Hz, 1H), 3.79−3.76 (m, 1H), 3.66−3.55 (m, 3H), 2.54 (d, J = 4.0 Hz, 3H), 2.33 (s, 2H); ^{13}C NMR (125 MHz, DMSO-d_6) δ 171.05, 171.01, 157.6, 154.8, 148.7, 147.4, 137.8, 129.5, 121.3, 120.3, 114.5, 86.1, 84.5, 81.2, 68.9, 66.2, 65.4, 61.3, 35.1, 25.0. HRMS m/z calcd for $C_{22}H_{26}N_6NaO_8$ $[M + Na]^+$ 525.1710, found 525.1715.

5′-*O*-(4,4′-Dimethoxytrityl)-2′-*O*-[2-(*N*-methylcarbamoyl)-ethyl]-2-*N*-phenoxyacetylguanosine (40). To a solution of compound **30** (330 mg, 0.66 mmol) in pyridine (6 mL) was added DMTrCl (244 mg, 0.72 mmol). The solution was stirred at ambient temperature for 3 h. The solution was diluted with $CHCl_3$ and extracted with saturated $NaHCO_3$ aq. The organic layer was dried, collected over sodium sulfate, and concentrated under reduced pressure. The residue was chromatographed on silica gel. Elution with TEA/MeOH/$CHCl_3$ (0.5:2:98, v/v/v) gave compound **40** (401 mg, 0.50 mmol, 75%): ^{1}H NMR (500 MHz, DMSO-d_6) δ 11.95−11.85 (m, 2H), 8.13 (s, 1H), 7.89 (d, J = 4.5 Hz, 1H), 7.36−7.21 (m, 11H), 7.00−6.97 (m, 3H), 6.85−6.82 (m, 4H), 5.92 (d, J = 5.5 Hz, 1H), 5.36 (d, J = 4.5 Hz, 1H, diminished with D_2O), 4.86 (dd, J = 15.5, 22.5 Hz, 2H), 4.50 (dd, J = 5.5, 10.0 Hz, 1H), 4.39−4.36 (m, 1H), 4.05−4.04 (m, 1H), 3.84−3.82 (m, 1H), 3.76−3.68 (m, 7H), 3.30−3.27 (m, 1H), 3.17−3.15 (m, 1H), 2.55 (d, J = 4.5 Hz, 3H), 2.38−2.34 (m, 2H); ^{13}C NMR (125 MHz, DMSO-d_6) δ 172.42, 170.78, 158.49, 156.97, 148.39, 144.44, 137.31, 135.53,

135.48, 130.00, 129.61, 128.08, 127.80, 126.88, 122.16, 121.26, 114.64, 114.53, 113.12, 86.50, 84.19, 82.24, 69.67, 66.94, 66.18, 63.34, 60.33, 55.12, 45.98, 35.61, 26.22, 14.12, 9.03. HRMS *m/z* calcd for $C_{43}H_{45}N_6O_{10}$ $[M + H]^+$ 805.3119, found 805.3112.

5′-*O*-(4,4′-Dimethoxytrityl)-2′-*O*-[2-(*N*-methylcarbamoyl)-ethyl]-2-*N*-phenoxyacetylguanosine-3′-(2-cyanoethyl *N,N*-diisopropylphosphoramidite) (23). To a solution of compound **40** (500 mg, 0.62 mmol) in dry MeCN (50 mL) were added 2-cyanoethyl-*N,N,N′,N′*-tetraisopropylphosphordiamidite (477 μL, 1.49 mmol) and diisopropylammonium 1*H*-tetrazolide (64 mg, 0.37 mmol). The solution was stirred at ambient temperature for 18 h. The solution was concentrated under reduced pressure. The residue was chromatographed on silica gel. Elution with 2% MeOH in $CHCl_3$ gave compound **23** (498 mg, 0.49 mmol, 80%): ^{1}H NMR (500 MHz, DMSO-d_6) δ 7.91−7.87 (m, 1H), 7.47−7.26, (m, 13H), 7.23−7.20, (m, 1H), 7.07−7.04 (m, 1H), 6.99−6.95 (m, 2H), 6.83−6.80 (m, 2H), 6.16−6.00 (m, 1H), 5.99−5.93 (m, 1H), 4.74−4.70 (m, 2H), 4.46−3.84 (m, 3H), 3.78−3.77 (m, 6H), 3.67−3.32 (m, 4H), 2.74−2.73 (m, 3H), 2.66−2.35 (m, 5H), 1.29−1.00 (m, 12H). HRMS *m/z* calcd for $C_{52}H_{61}N_8O_{11}PNa$ $[M + Na]^+$ 1027.4095, found 1027.4098.

Oligonucleotide Synthesis. RNA oligonucleotides (Table 2) were synthesized on an Applied Biosystems 392 oligonucleotide synthesizer on a 1 μmol scale, using a 0.1 M solution each of **20**, **21**, **22**, and **23** with commercially available 5′-*O*-(4,4′-dimethoxytrityl)-2′-*O*-methyl-3′-*O*-(2-cyanoethyl-*N,N*-diisopropylphosphoramidite monomers of uridine, 4-*N*-benzoylcytidine, 6-*N*-benzoyladenosine (ABz), and 2-*N*-isobutyrylguanosine (GiBu). A 0.25 M solution of 5-ethiothio-1*H*-tetrazole in dry acetonitrile or a 0.25 M solution of 5-(bis-3,5-trifluoromethylphenyl)-1*H*-tetrazole in dry acetonitrile was used as the activator for the coupling reaction. Coupling time was set to be 10 min. [(Dimethylaminomethylidene)amino]-3*H*-1,2,4-dithiazole-3-thione (DDTT)[42] was used as the sulfurization agent for the phosphorothioate synthesis. After completion of the synthesis, the release of 2′-*O*-modified oligonucleotides from the support and deprotection of all protecting groups were simultaneously carried out in NH_4OH (1 mL) at ambient temperature for 2 h, and then CPG was filtrated. The filtrate was heated at 55 °C for 5 h. The filtrate was concentrated under reduced pressure and then subjected to C-18 cartridge purification. Each product was purified by using anion-exchange chromatography.

T_m Experiments. Each oligonucleotide (1.0 nmol) was dissolved in 10 mM sodium phosphate buffer (pH 7.0, containing 150 mM NaCl and 0.1 mM EDTA) (500 μL) to arrange the final concentration of each oligonucleotide to be 2 μM. The solution was separated into quartz cells (10 mm) and incubated at 85 °C. After 10 min, the solution was cooled to 5 °C at a rate of annealing and melting, the absorption at 260 nm was recorded and used to draw UV-melting curves. T_m values were calculated as the temperature that gave the maximum of the first derivative of the UV−melting curve.

Nuclease Resistance Assay. Each oligonucleotide (10.0 nmol) was dissolved in Tris-HCl buffer (at pH 8.5, 72 mM NaCl, 14 mM $MgCl_2$ at 37 °C) (990 μL). To the solution was added snake venom phosphodiesterase (5×10^{-4} unit/mL) (10 μL) to arrange the final concentration of each oligonucleotide to be 10 μM. Aliquots of the reaction solution were removed at indicated times, quenched by heating at 100 °C for 2 min. The mixture was analyzed by anion exchange HPLC.

Delivery Method. Eight weeks old *mdx52* mice were used. As antisense oligonucleotides against exon 51 of dystrophin gene, ORNs 9−12 were used. Each antisense oligonucleotide (20 μg) was dissolved in saline. Ten micrograms of antisense oligonucleotide was injected into each tibialis anterior muscle with lipofectamine 2000. Two weeks after injection, mice were sacrificed and muscles were dissected. Total RNA was extracted from frozen tissue and 50 ng of total RNA was used for one-step RT-PCR according to the manufacturer's instructions. The primer sequences were Ex50F 5′-TTTACTTCGGGAGCTGAGGA-3′ and Ex53R 5′-ACCTGTTCGGCTTCTTCCTT-3′ for amplification of cDNA from exons 50−53. The PCR conditions were 95 °C for 4 min, then 35 cycles of 94 °C for 1 min, 60 °C for 1 min, 72 °C for 1 min, and finally 72 °C for 7 min. The intensity of PCR bands was analyzed by using ImageJ software (http://rsbweb.nih.gov/ij/), and skipping efficiency was calculated by using the following formula [(the intensity of skipped band)/(the intensity of skipped band + the intensity of unskippedband)], after the resulting PCR bands were extracted using a gel extraction kit.

Immunohistochemistry. Eight micrometer cryosections were cut from flash-frozen muscle, then placed on poly-L-lysine-coated slides and air-dried. The sections were stained with monoclonal mouse antibody *Dys*-2 against C-terminus of cardiac muscular dystrophin from normal mouse used as a secondary antibody. 4′,6-Diamidino-2-phenylindole containing a mounting agent was used for nuclear counterstaining.

■ ASSOCIATED CONTENT

Supporting Information. ^{1}H NMR, ^{13}C NMR, and ^{31}P NMR charts. This material is available free of charge via the Internet at http://pubs.acs.org.

■ AUTHOR INFORMATION

Corresponding Author
*Email: msekine@bio.titech.ac.jp.

■ ACKNOWLEDGMENT

This work was supported by a Grant-in-Aid for Scientific Research from the Ministry of Education, Culture, Sports, Science and Technology, Japan, and in part by Health Sciences Research Grants for Research on Psychiatric and Neurological Diseases and Mental Health from the Ministry of Health, Labor and Welfare of Japan and the global COE project.

■ REFERENCES

(1) Jackson, A. L.; Burchard, J.; Leake, D.; Reynolds, A.; Schelter, J.; Guo, J.; Johnson, J. M.; Lim, L.; Karpilow, J.; Nichols, K.; Marshall, W.; Khvorova, A.; Linsley, P. S. *RNA* **2006**, *12*, 1197–1205.

(2) Manoharan, M. *Antisense Nucleic Acid Drug Dev.* **2002**, *12*, 103–128.

(3) Ge, Q.; Dallas, A.; Ilves, H.; Shorensten, J.; Behlke, M. A.; Johnston, B. H. *RNA* **2010**, *16*, 118–130.

(4) Burmeister, P. E.; Lewis, S. D.; Silva, R. F.; Preiss, J. R.; Horwitz, L. R.; Pendergrast, P. S.; McCauley, T. G.; Kurz, J. C.; Epstein, D. M.; Wilson, C.; Keefe, A. D. *Chem. Biol.* **2005**, *12*, 25–33.

(5) Inoue, H.; Hayase, Y.; Imura, A.; Iwai, S.; Miura, K.; Ohtsuka, E. *Nucleic Acids Res.* **1987**, *15*, 6131–48.

(6) Yu, R. Z.; Geary, R. S.; Monteith, D. K.; Matson, J.; Truong, L.; Fitchett, J.; Levin, A. A. *J. Pharm. Sci.* **2004**, *93*, 48–59.

(7) Griffey, R. H.; Monia, B. P.; Cummins, L. L.; Freier, S.; Greig, M. J.; Guinosso, C. J.; Lesnik, E.; Manalili, S. M.; Mohan, V.; Owens, S.; Ross, B. R.; Sasmor, H.; Wancewicz, E.; Weiler, K.; Wheeler, P. D.; Cook., P. D. *J. Med. Chem.* **1996**, *39*, 5100–5109.

(8) Prakash, T. P.; Kawasaki, A. M.; Wancewicz, E. V.; Shen, L.; Monia, B. P.; Ross, B. S.; Bhat, B.; Manoharan, M. *J. Med. Chem.* **2008**, *51*, 2766–2776.

(9) Bumcrot, D.; Manoharan, M.; Koteliansky, V.; Sah, D. W. Y. *Nat. Chem. Biol.* **2006**, *2*, 711–719.

(10) Geary, R. S.; Watanabe, T. A.; Truong, L.; Freier, S.; Lesnik, E. A.; Sioufi, N. B.; Sasmor, H.; Manoharan, M.; Levin, A. A. *J. Pharmacol. Exp. Ther.* **2001**, *296*, 890–897.

(11) Freier, S. M.; Altmann, K.-H. *Nucleic Acids Res.* **1997**, *15*, 4429–43.
(12) Manoharan, M.; Tivel, K. L.; Cook, P. D. *Tetrahedron Lett.* **1995**, *36*, 3651–3654.
(13) Sakamoto, T.; Kobori, A.; Murakami, A. *Bioorg. Med. Chem. Lett.* **2008**, *18*, 2590–2593.
(14) Winkler, J.; Gilbert, M.; Kocourkova, A.; Stessl, M.; Noe, C. R. *ChemMedChem* **2008**, *3*, 102–110.
(15) (a) Ross, B. S.; Springer, R. H.; Tortorici, Z.; Dimock, S. *Nucleosides Nucleotides* **1997**, *16*, 1641–1643. (b) Oeda, Y.; Iijima, Y.; Taguchi, H.; Ohkubo, A.; Seio, K.; Sekine, M. *Org. Lett.* **2009**, *11*, 5582–5585.
(16) Sivets, G. G. *Nucleosides Nucleotides Nucleic Acids* **2007**, *26*, 1237–1240.
(17) Saneyoshi, H.; Seio, K.; Sekine, M. *J. Org. Chem.* **2005**, *70*, 10453–10460.
(18) Saneyoshi, H.; Ando, K.; Seio, K.; Sekine, M. *Tetrahedron* **2007**, *63*, 11195–11203.
(19) Sekine, M. *J. Org. Chem.* **1989**, *54*, 2321–2326.
(20) (a) Urata, H.; Hara, H.; Hirata, Y.; Ohmoto, N.; Akagi, M. *Nucleic Acids Symp. Ser.* **1985**, *16*, 165–168. (b) Markiewicz, W. T. *J. Chem. Res., Miniprint* **1979**, 173.
(21) Pon, R. T.; Yu, S.; Prabhavalkar, T.; Mishra, T.; Kulkarni, B.; Sanghvi, Y. S. *Nucleosides Nucleotides Nucleic Acids* **2005**, *24*, 777–781.
(22) Robins, M. J.; Hansske, F.; Bernier, S. E. *Can. J. Chem.* **1981**, *59*, 3360–3364.
(23) Grotli, M.; Douglas, M.; Beijer, B.; Garcia, G.; Eritja, R.; Sproat, B. *J. Chem. Soc., Perkin Trans. 1* **1997**, *18*, 2779–2788.
(24) Beigelman, L.; Haeberli, P.; Sweedler, D.; Karpeisky, A. *Tetrahedron* **2000**, *56*, 1047–1057.
(25) Sanger, W. *Principles of Nucleic Acid Structure*; Springer: New York, 1984.
(26) Bordwell, F. G.; Algrim, D.; Vanier, N. R. *J. Org. Chem.* **1977**, *42*, 1817–1819.
(27) Velikyan, I.; Acharya, S.; Trifonova, A.; Foeldesi, A.; Chattopadhyaya, J. *J. Am. Chem. Soc.* **2001**, *123*, 2893–2894.
(28) Nielsen, J.; Taagaard, M.; Marugg, J. E.; van Boom, J. H.; Dahl, O. *Nucleic Acids Res.* **1986**, *14*, 7391–7403.
(29) Wu, X.; Pitsch, S. *Nucleic Acids Res.* **1998**, *26*, 4315–4323.
(30) Leuck, M.; Wolter, A. *PCT Int. Appl.* 2006, WO 2006116476 A1 20061102.
(31) Overhoff, M.; Sczakiel, G. *EMBO Rep* **2005**, *6*, 1176–1181.
(32) Shaw, J.-P.; Kent, K.; Bird, J.; Fishback, J.; Froehler, B. *Nucleic Acids Res.* **1991**, *19*, 747–750.
(33) Aartsma-Rus, A.; van Ommen, G.-J. B. *RNA* **2007**, *13*, 1609–1624.
(34) Lu, Q. L.; Rabinowitz, A.; Chen, Y. C.; Yokota, T.; Yin, H.; Alter, J.; Jadoon, A.; Bou-Gharios, G.; Partridge, T. *Proc. Natl. Acad. Sci. U.S.A.* **2005**, *102*, 198–203.
(35) Crooke, S. T.; Graham, M. J.; Zuckerman, J. E.; Brooks, D.; Conklin, B. S.; Cummins, L. L.; Greig, M. J.; Guinosso, C. J.; Kornbrust, D.; Manoharan, M.; Sasmor, H. M.; Schleich, T.; Tivel, K. L.; Griffey, R. H. *J. Pharmacol. Exp. Ther.* **1996**, *277*, 923–937.
(36) Marcusson, E. G.; Bhat, B.; Manoharan, M.; Bennett, C. F.; Dean, N. M. *Nucleic Acids Res.* **1998**, *26*, 2016–2023.
(37) Arechavala-Gomeza, V.; Graham, I. R.; Popplewell, L. J.; Adams, A. M.; Aartsma-Rus, A.; Kinali, M.; Morgan., J. E.; Van Deutekom, J. C.; Wilton, S. D.; Dickson, G.; Muntoni, F. *Hum. Gene Ther.* **2007**, *18*, 798–810.
(38) Ciccarone, V.; Chu, Y.; Schifferli, K.; Pichet, J.-P.; Hawley-Nelson, P.; Evans, K.; Roy, L.; Bennett, S. *FOCUS* **1999**, *21*, 2.
(39) Araki, E.; Nakamura, K.; Nakao, K.; Kameya, S.; Kobayashi, O.; Nonaka, I.; Kobayashi, T.; Katsuki, M. *Biochem. Biophys. Res. Commun.* **1997**, *238*, 492–497.
(40) Beaucage, S. L.; Caruthers, M. H. *Tetrahedron Lett.* **1981**, *22*, 1859–1862.
(41) Nielsen, J.; Taagaard, M.; Marugg, J. E.; van Boom, J. H.; Dahl, O. *Nucleic Acids Res.* **1986**, *14*, 7391–7403.
(42) Overhoff, M.; Sczakiel, G. *EMBO Rep.* **2005**, *6*, 1176–1181.

NOTE ADDED AFTER ASAP PUBLICATION

This paper was published to the Web on March 23, 2011, with errors in schemes 1 and 3. These errors were fixed when the paper was published to the Web on March 29, 2011.

OPEN ACCESS Freely available online

PLoS one

Identification of Muscle-Specific MicroRNAs in Serum of Muscular Dystrophy Animal Models: Promising Novel Blood-Based Markers for Muscular Dystrophy

Hideya Mizuno[1], Akinori Nakamura[2], Yoshitsugu Aoki[2,4], Naoki Ito[2,5], Soichiro Kishi[1], Kazuhiro Yamamoto[3], Masayuki Sekiguchi[3], Shin'ichi Takeda[2], Kazuo Hashido[1]*

1 Administrative Section of Radiation Protection, National Institute of Neuroscience, National Center of Neurology and Psychiatry, Kodaira, Tokyo, Japan, **2** Department of Molecular Therapy, National Institute of Neuroscience, National Center of Neurology and Psychiatry, Kodaira, Tokyo, Japan, **3** Department of Degenerative Neurological Diseases, National Institute of Neuroscience, National Center of Neurology and Psychiatry, Kodaira, Tokyo, Japan, **4** Department of System Neuroscience, Medical Research Institute, Tokyo Medical and Dental School University Graduate School, Tokyo, Japan, **5** Department of Biological Information, Tokyo Institute of Technology, Yokohama, Japan

Abstract

Duchenne muscular dystrophy (DMD) is a lethal X-linked disorder caused by mutations in the *dystrophin* gene, which encodes a cytoskeletal protein, dystrophin. Creatine kinase (CK) is generally used as a blood-based biomarker for muscular disease including DMD, but it is not always reliable since it is easily affected by stress to the body, such as exercise. Therefore, more reliable biomarkers of muscular dystrophy have long been desired. MicroRNAs (miRNAs) are small, ~22 nucleotide, noncoding RNAs which play important roles in the regulation of gene expression at the post-transcriptional level. Recently, it has been reported that miRNAs exist in blood. In this study, we hypothesized that the expression levels of specific serum circulating miRNAs may be useful to monitor the pathological progression of muscular diseases, and therefore explored the possibility of these miRNAs as new biomarkers for muscular diseases. To confirm this hypothesis, we quantified the expression levels of miRNAs in serum of the dystrophin-deficient muscular dystrophy mouse model, *mdx*, and the canine X-linked muscular dystrophy in Japan dog model ($CXMD_J$), by real-time PCR. We found that the serum levels of several muscle-specific miRNAs (miR-1, miR-133a and miR-206) are increased in both *mdx* and $CXMD_J$. Interestingly, unlike CK levels, expression levels of these miRNAs in *mdx* serum are little influenced by exercise using treadmill. These results suggest that serum miRNAs are useful and reliable biomarkers for muscular dystrophy.

Citation: Mizuno H, Nakamura A, Aoki Y, Ito N, Kishi S, et al. (2011) Identification of Muscle-Specific MicroRNAs in Serum of Muscular Dystrophy Animal Models: Promising Novel Blood-Based Markers for Muscular Dystrophy. PLoS ONE 6(3): e18388. doi:10.1371/journal.pone.0018388

Editor: Sebastien Pfeffer, French National Center for Scientific Research - Institut de biologie moléculaire et cellulaire, France

Received October 27, 2010; **Accepted** March 6, 2011; **Published** March 30, 2011

Funding: This work was supported by the Health and Labour Sciences Research Grants for Translational research from the ministry of Health, Labour and Welfare of Japan. The funders had no role in study design, data collection and analysis, decision to publish, or preparation of the manuscript.

Competing Interests: The authors have declared that no competing interests exist.

* E-mail: hashido@ncnp.go.jp

Introduction

Duchenne muscular dystrophy (DMD) is a lethal X-linked disorder caused by mutations in the *dystrophin* gene, which encodes a cytoskeletal protein, dystrophin[1]. The absence of dystrophin results in progressive degeneration of skeletal and cardiac muscle with fibrotic tissue replacement, fatty infiltration, and subsequent early death by respiratory or heart failure[2,3]. Creatine kinase (CK) is an enzyme related to energy metabolism present in various types of cells[4]. CK is commonly used as a blood-based biomarker for muscular dystrophy to evaluate the level of muscle damage and necrosis, and the efficacy of potential therapies, but it is not always reliable since it is easily affected by stress to the body, such as exercise[5,6,7]. Other markers for muscular dystrophy, such as myoglobin, aldolase or lactate dehydrogenase, also have the same problem. Therefore, more reliable biomarkers of muscular dystrophy have long been desired.

MicroRNAs (miRNAs) are small, ~22 nucleotide, noncoding RNAs which play important roles in the regulation of gene expression at the post-transcriptional level[8]. Recently, it has been reported that specific miRNAs in blood are promising biomarkers for cancer, liver injury and heart failure [9,10,11]. These studies showed that the levels of specific circulating miRNAs are associated with the development of these pathological processes. It has also been reported that miRNAs are released from cells through an exosomal-mediated pathway[12], suggesting that circulating miRNAs are packaged in exosomes, which protects them from RNases.

We hypothesized that the expression levels of specific serum circulating miRNAs may be useful to monitor the pathological progression of muscular diseases, and therefore explored the possibility of these miRNAs as new biomarkers for muscular diseases. Here, we demonstrate that the serum levels of several muscle-specific miRNAs are increased in the dystrophin-deficient muscular dystrophy mouse model, *mdx*, as well as the canine X-linked muscular dystrophy in Japan dog model ($CXMD_J$) [13,14,15]. These results suggest that serum miRNAs are useful as markers for muscular dystrophy.

Results

To explore the possibility of miRNA as a biomarker for DMD, we quantified the expression levels of several miRNAs in the serum

of *mdx* by real-time PCR. The expression levels of miRNAs are indicated as either cycle threshold (Ct) (**Figure 1a**) or fold expression compared to wild-type (**Figure S1**). The Ct values of the ubiquitously expressed miR-16, brain-rich miR-132 [16] and small nucleolar RNA 202 (sno202) did not show any significant differences between wild-type and *mdx* serum (**Figure 1a**). In contrast, muscle-specific miR-1, -133a and -206 [17,18,19] were significantly increased in *mdx* (**Figure 1a**). The expression levels of these miRNAs in *mdx* were 10- to 100-fold higher than in wild-type controls (**Figure S1**). In Figure 1, the data are shown without normalization by an internal control RNA. Although small nuclear RNA U6, sno202 and ubiquitously expressed miRNA, such as miR-16, are often used as an internal control for miRNA analysis, there is currently no consensus for a serum internal control miRNA for real-time PCR analysis. Indeed, we examined the expression of U6 but found it was undetectable in serum (data not shown), and sno202 and miR-16 revealed no significant difference between wild-type and *mdx* (**Figure 1a** and **Figure S1**). In addition, miR-16 was more abundant than sno202 in serum (**Figure 1a**). Therefore, we employed miR-16 as the internal control for normalization of muscle-specific miRNAs in serum in the subsequent studies.

We also confirmed the accuracy of miR-16 as an internal control by using exogeneous miRNA (spiked-in miRNA). *C. elegans* miRNA-39 (cel-miR-39) was used as a spiked-in miRNA because of the lack of sequence homology to mouse miRNAs. Synthetic cel-miR-39 was spiked into serum after the addition of denaturing solution including RNase inhibitors. Then, miRNAs were isolated and the levels of cel-miR-39, miR-16, -1, -133a and -206 were determined by real-time PCR (**Figure S2**). In three-repeated experiments, the quantities of cel-miR-39 and miR-16 showed similar levels each time (**Figure S2a**). Furthermore, the expression levels of miR-1, -133a and -206 were calculated by normalization with cel-miR-39 or miR-16, individually (**Figure S2b**). The expression levels of miR-1, -133a and -206 were highly elevated in *mdx*, and the results were consistent between normalization with cel-miR-39 and miR-16.

It is conceivable that leakage or secretion from skeletal muscle fibers is the major cause of the increase in muscle-specific miRNAs in serum, but there remains the possibility that these miRNAs are excessively expressed in dystrophic skeletal muscle, which then influences serum expression levels. To investigate this possibility, we examined the expression level of these miRNAs in the skeletal muscle (soleus: Sol, tibialis anterior: TA and diaphragm: DIA) of *mdx* (**Figure S3**). Levels of ubiquitously expressed miR-16 were not different among the muscles examined, but miR-1 and miR-133a were significantly decreased in Sol and TA of *mdx*, although the differences are less than 2-fold. On the other hand, miR-206 was significantly increased in *mdx* TA and DIA, but not in Sol, and this increase of miR-206 in some *mdx* muscles could be related to a previously reported role for miR-206 in muscle regeneration[20]. Since miR-1 and -133a levels were highly elevated in *mdx* serum, although they were not increased in *mdx* skeletal muscle, suggests that the increase of muscle-specific miRNAs in *mdx* serum is caused by an increase in leakage or secretion of miRNAs from muscle.

Since it is very important to investigate whether muscle-specific miRNA levels are affected by exercise like as CK, we compared CK and miRNA levels in mice serum after exercise using a treadmill. Both CK and miRNA were increased after the treadmill exercise (**Figure 1b**, left, normalized to wild-type control), however miRNAs appeared to be less affected. When the increase in miRNAs were corrected by the data before exercise in each group (**Figure 1b**, right, normalized by each control), CK showed almost a 60-fold increase after exercise, whereas the change of muscle-specific miRNA levels was less than 10-fold.

$CXMD_J$ is a well characterized dog model of DMD, which shows severe and progressive symptoms[13,14,15]. We therefore analyzed the expression levels of miRNAs in normal, carrier (females possessing a mutant *dystrophin* gene on one of two X-chromosomes) and $CXMD_J$ dog serum at various ages. The Ct value of these miRNAs in $CXMD_J$ was significantly smaller than age-matched controls (**Figure S4**). Relative expression levels corrected by miR-16 are shown in **Figure 2**. These miRNAs are apparently able to distinguish $CXMD_J$ from age-matched normal dogs. Shimatsu *et al.* previously reported that the CK concentration of $CXMD_J$ dogs do not increase with age [21]. Thus, our results of these miRNA levels are consistent with the CK levels in this model.

Our data indicate that the levels of miR-1, -133a and -206 relative to miR-16 are increased in the serum of two animal models of muscular dystrophy, *mdx* and $CXMD_J$. It is very intriguing that serum miRNA were less affected by stress, such as exercise, compared with CK. In conclusion, muscle-specific miRNAs in serum may be useful biological markers for muscular dystrophy which are more reliable than CK, and further investigations are required to clarify the molecular mechanisms by which miRNAs are released from the inside of cells into serum.

Discussion

Recently, several studies have reported that miRNAs in serum are promising biomarkers for diseases, such as cancers, liver injury or heart failure [9,10,11]. CK is commonly used as a biomarker of muscular diseases to evaluate the level of muscle damage and necrosis, and the efficacy of potential therapies, but it is not always reliable since it is easily affected by stress to the body, such as exercise [5,6,7]. Therefore, more reliable biomarkers of muscular dystrophy have long been desired. We hence investgigated whether serum miRNAs are useful for monitoring the pathological condition of muscular diseases. In this report, we demonstrate that the serum levels of several muscle-specific miRNAs are increased in two dystrophin-deficient muscular dystrophy animal models. Importantly, we show that the levels of these miRNAs are much less affected by stress to the body compared with CK levels.

To investigate the mechanism of the increase of miRNA expression, we also examined the expression level of miR-1, miR-133a and miR-206 in the skeletal muscle of *mdx* (**Figure S3**). miR-1 and -133a were significantly decreased in Sol and TA of *mdx*. On the other hand, miR-206 was significantly increased in TA and DIA of *mdx*. Our results suggest that the increase of muscle-specific miRNAs in the serum of these DMD models is caused by an increase in leakage or secretion of miRNAs from muscle, and not by the change of expression in skeletal muscle. However, it is not yet clear whether the increase of these miRNAs is caused by leakage or secretion from muscle. It is conceivable that leakage from skeletal muscle fibers is the major cause of the increase in muscle-specific miRNAs in mdx serum, but it is hard to explain why these miRNAs were not degraded by RNase. Mitchell *et al.* [10] showed that synthetic miRNAs are immediately degraded in serum even though endogenous circulating miRNAs are stably expressed in serum. To explain these results, they suggested that miRNAs are released from cells through an exosomal-mediated pathway. If circulating miRNAs are secreted by an exosomal-mediated pathway, it is possible that dystrophin is involved in the regulation of exosome secretion and a lack of dystrophin results in increased miRNA release. However, further investigation is required to clarify the contribution of dystrophin in exosome secretion.

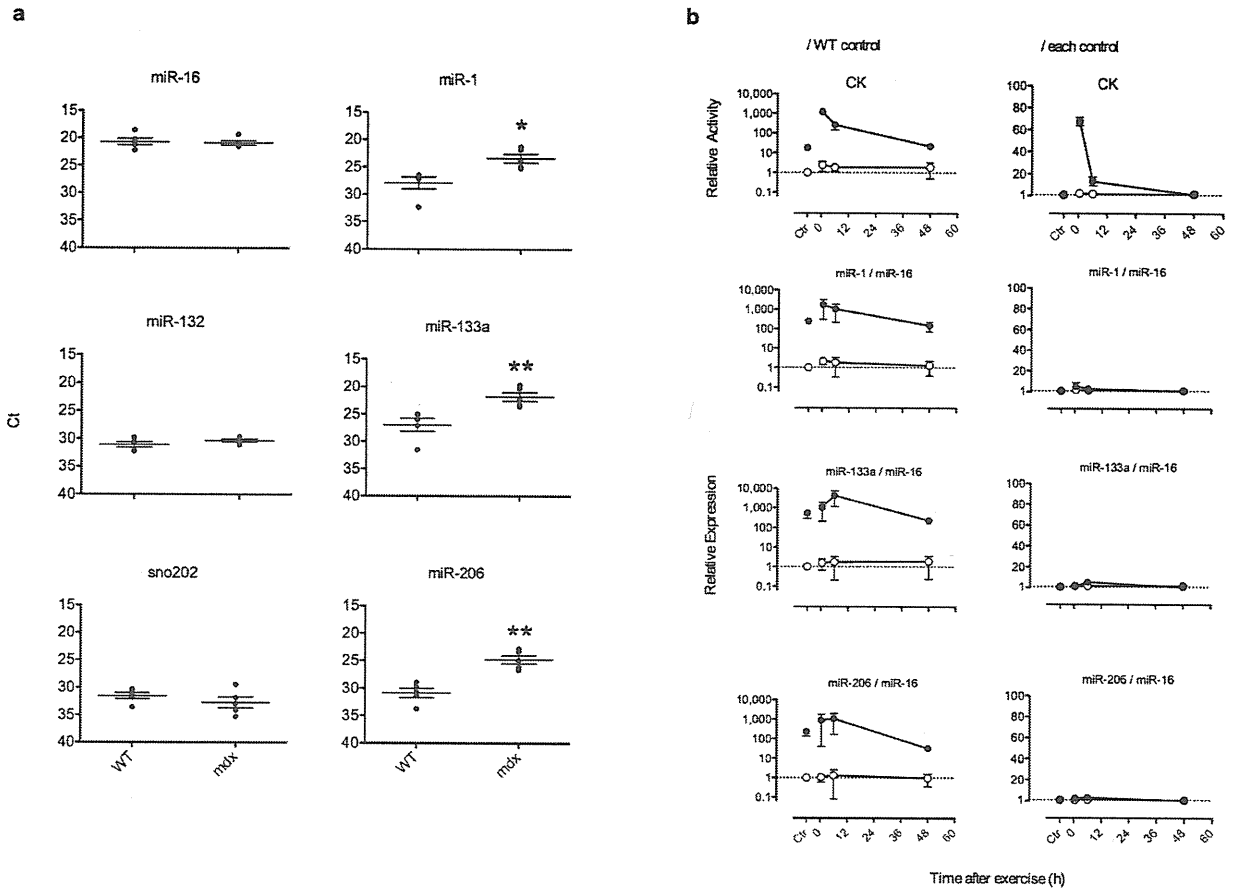

Figure 1. Elevation of muscle-specific miRNA levels in *mdx* mouse serum. (a) Expression levels of miRNAs in 8-week old male wild-type and *mdx* serum. Ct was determined by real-time PCR. In these graphs, the longer bars on each plot indicate the mean, and the shorter bars indicate ± SEM, n = 5. Asterisk (*) indicates a significant difference (*, $P<0.05$; **, $P<0.01$, two-tailed Student's t-test.). The actual P value for each test was P = 0.797 (miR-16), 0.222 (miR-132), 0.344 (sno202), 0.011 (miR-1), 0.007 (miR-133a) and 0.001 (miR-206). (b) CK and miRNA expression levels in wild-type and *mdx* serum after treadmill exercise. Running on the treadmill was continued for 20 min. About 100 μl of blood was collected from the tail vein at 0.5, 6 and 48 h after the exercise. Six days before the test, blood was collected as a control. Expression levels were normalized to the wild-type control (left) or each individual control (right). Data are presented as mean ± SEM, n = 3. ○: wild-type; ●: *mdx*.
doi:10.1371/journal.pone.0018388.g001

The change of miRNA expression levels in skeletal muscle of *mdx* in this report is consistent with previous reports [20,22]. It is intriguing that TA muscle of denervated mice also showed an increase in miR-206 and a decrease in miR-1 and -133a [23]. Yuasa *et al.* [20] also showed that miR-206 expression was increased after cardiotoxin-induced muscle regeneration and that miR-206 contributes to muscle regeneration. Interestingly, it has been showed that the expression levels of miR-206 in DMD patients are not increased [24] or that the increase is not as large as in *mdx* [22]. Although *mdx* mice are deficient in dystrophin, they do not show lethality unlike in humans. Increased miR-206 expression levels in *mdx* therefore contribute to the different phenotype between humans and mice. In addition, Williams *et al.* [23] showed that expression of miR-206 delayes disease progression and promotes regeneration of neuromuscular synapses in amyotrophic lateral sclerosis (ALS) model mice. Taken together, these results indicate that gene therapy using miR-206 may be a useful treatment for muscular diseases.

In this report, we focused on muscle-specific miRNAs and found that they are significantly increased in serum of DMD models. To investigate whether such an increase can be observed in some myopathy models which do not have any effective diagnosis markers, we also measured these muscle-specific miRNAs in serum of steroid treated dogs. We found that serum level of miR-1, -133a and -206 were not increased in steroid treated dog did not show increase compared with non-treatment controls (data not shown). Intriguingly, *Lodes et al.* [25] performed microarray analysis with circulating miRNAs and found an increase in specific miRNAs in serum of cancer patients. Furthermore the miRNA expression patterns were able to discriminate between healthy controls and cancer patients. Such a microarray analysis may be useful for identifying diagnosis markers for muscular diseases for which effective diagnosis markers currently do not exist.

Materials and Methods

Ethics Statement

The dog study was approved by the Ethics Committee for the Treatment of Middle-sized Laboratory Animals of the National Institute of Neuroscience, National Center of Neurology and Psychiatry, approval ID: 21-02 and 22-02. The mice study was

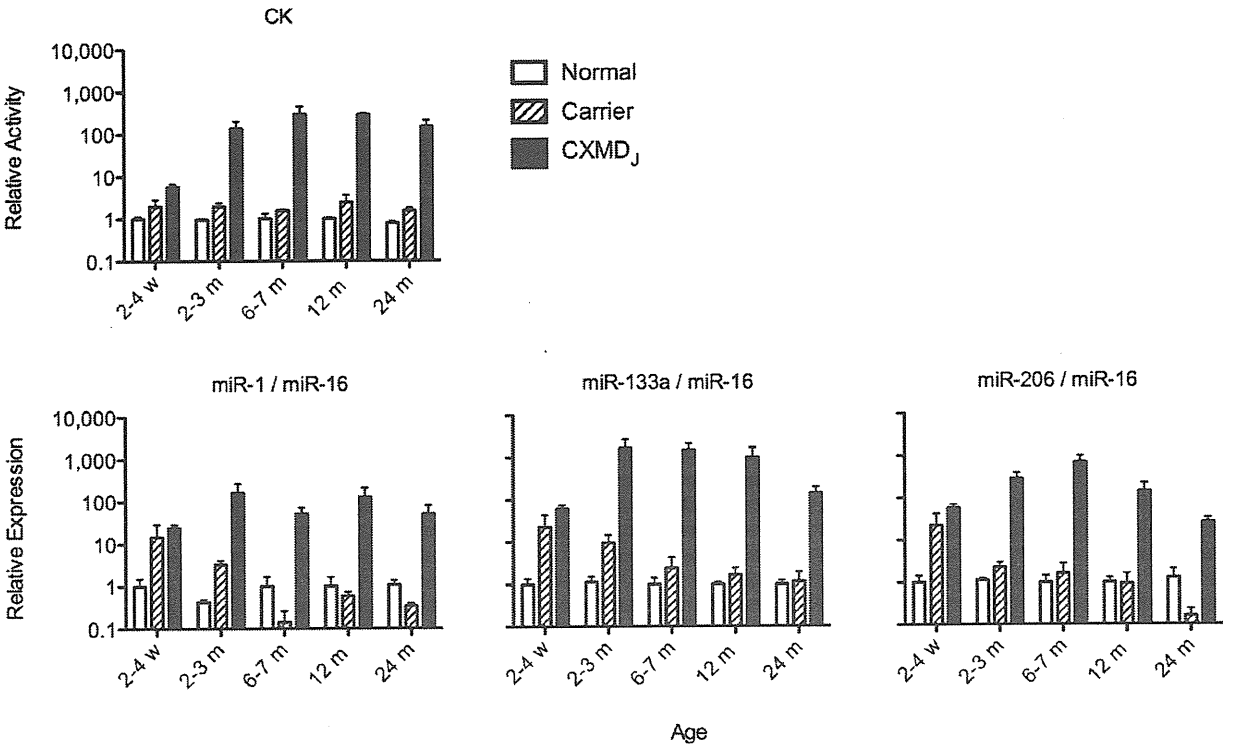

Figure 2. Elevation of muscle-specific miRNAs in CXMD$_J$ dog serum. CK activity and miRNA expression in the serum of normal, carrier and dystrophy dogs (CXMD$_J$) at the indicated ages were determined. Expression levels of miR-1, miR-133a, miR-206 and miR-16 were determined by real-time PCR, and levels of each muscle-specific miRNA (miR-1, miR-133a and miR-206) was corrected by miR-16 levels. Results are indicated as relative expression to normal dogs at each age, and are presented as mean ± SEM, n = 3. w: weeks; m: months.
doi:10.1371/journal.pone.0018388.g002

approved by the Ethics Committee for the Treatment of Laboratory Animals of the National Institute of Neuroscience, National Center of Neurology and Psychiatry, approval ID: 2008011.

Animals and serum samples

All animals in this study were cared for and treated in accordance with the guidelines provided by the Ethics Committee for the Treatment Laboratory Animals of National Institute of Neuroscience, or the Ethics Committee for the Treatment Laboratory Middle-sized Animals of National Institute of Neuroscience. Skilled experimental animal technicians, who have special knowledge of methods to prevent unnecessary excessive pain, handled the animals and assisted in the experiments.

As Duchenne muscular dystrophy (DMD) models, the X-chromosome-linked muscular dystrophy (*mdx*) mouse and canine X-linked muscular dystrophy in Japan (CXMD$_J$), Beagle-based medium-sized dystrophic dogs, were used in this study. In **Figure 1a**, whole body blood of male *mdx* mice (n = 5) or age-matched controls (strain C57BL/10; B10) (n = 5) at 8 weeks were collected from the abdominal vena cava under anesthesia. Blood collection after the treadmill test (**Figure 1b**), was performed from the tail vein of *mdx* (n = 3) or age-matched control (n = 3) under anesthesia. The phenotype of CXMD$_J$ has been reported previously[13,14,15]. For analysis of the serum of CXMD$_J$ dogs, mutation carrier female dogs and wild-type control dogs (n = 3, at each age indicated in Figure 2), blood was collected from the subcutaneous vein of the hindlimb, and whole blood was allowed to stand for about 1 h at room temperature before centrifugation at 1,800 g for 10 min at room temperature. The resultant serum was dispensed into a 1.5 ml cryotube and stored at −80°C until use.

RNA isolation and quantification of miRNA

Total RNA, including miRNA, was extracted from 50 µl of serum using the mirVana miRNA isolation kit (Ambion, Austin, TX, USA) according to the manufacturer's instructions, and finally eluted with 50 µl of elution buffer provided by the manufacturer. Five µl of total RNA was reverse transcribed using the TaqMan miRNA Reverse Transcription kit (Applied Biosystems, Foster City, CA, USA) and miRNA-specific stem-loop primers (part of TaqMan miRNA assay kit; Applied Biosystems). The expression levels of miRNA were quantified by real-time PCR using individual miRNA-specific primers (part of TaqMan miRNA assay kit; Applied Biosystems) with 7900HT Fast Real-Time PCR System (Applied Biosystems) according to the manufacturer's instructions. There is no current consensus on the use of an internal control for real-time PCR analysis of serum miRNA. Therefore, we used fixed volumes of starting serum (50 µl), buffer for the elution of RNA (50 µl) from starting serum, and input into the RT reaction (5 µl) in each assay for technical consistency. Data analysis was performed by SDS 2.1 real-time PCR data analysis software (Applied Biosystems). Threshold was fixed at 0.2 in each analysis for data consistency. The similarities of linearity of primers for each target miRNA were confirmed by using a dilution series of synthetic miRNAs.

Spiked-in miRNA experiment

We followed the protocol previously reported by Mitchell *et al.* [10] to determine endogenous miRNA levels with spiked-in miRNA. Spiked-in miRNA was designed against *C. elegans* microRNA-39 (cel-miR-39)(5′-UCACCGGGUGUAAAUCAG-CUU-3′), and was synthesized by Sigma Aldrich Japan. Synthetic cel-miR-39 was spiked into serum after the addition of denaturing solution including RNase inhibitors. Isolation of total RNA, including miRNA, and quantification of the expression levels of miRNAs by real-time PCR were performed as described above.

Creatine kinase determination

Serum creatine kinase (CK) levels were assayed with the Fuji Drychem system (Fuji Film Medical Co. Ltd, Tokyo, Japan) according to the manufacturer's instructions. Data was expressed as units per liter (U/l).

Treadmill test

Mice were forced to run on a treadmill (MK-680S treadmill: Muromachi Kikai, Tokyo, Japan) with an inclination of 0° at 5 m/min for 5 min. Then, the speed was increased by 1 m/min every minute for a further 15 min. After the running, blood was immediately collected from the tail vein, as well as subsequently collected at the indicated times.

Statistics

Statistical significances between groups were determined by the two-tailed t-test, or one-way ANOVA with Bonferroni post hoc test. Each analysis was performed by Prism 5 (Graphpad Software Inc., San Diego, CA, USA).

Supporting Information

Figure S1 miRNA expression in 8-week old male wild-type control and *mdx* serum. Expression levels of miRNAs were determined by real-time PCR. Results are shown as relative expression, and data are presented as mean ± SEM, n = 5.
(TIFF)

Figure S2 (a) Confirmation of the consistency of miRNA isolation from serum. *C. elegans* miR-39 (cel-miR-39) was chemically synthesized and added to the denatured mouse serum samples. Total RNA was isolated from the mouse serum samples, and the quantity of exogenous cel-miR-39 and endogenous miR-16 were determined by real-time PCR. (b) Expression levels of miR-1, -133a and -206 in wild-type control and *mdx* serum, which were individually normalized by the cel-miR-39 spiked-in control or the endogenous control, miR-16. Results are shown as relative expression. The longer bars on each plot indicate the mean, and the shorter bars indicate ± SEM, n = 3.
(TIFF)

Figure S3 miRNA expression in wild-type control and *mdx* muscles. Expression levels of miR-1, -16, -133a and -206 in Soleus (Sol), tibialis anterior (TA) and diaphragm (DIA) were determined by real-time PCR. Results are shown as relative expression. sno202 was used as an internal control. Data are presented as mean ± SEM, n = 4. Asterisk (*) indicates a significant difference (*, $P<0.05$; $P<0.01$, two-tailed Student's t-test.). The actual P value for each test was $P = 0.024$ (miR-1) and 0.010 (miR-206) in Sol; $P = 0.002$ (miR-1), 0.008 (miR-133a) and <0.001 (miR-206) in TA; $P = 0.006$ (miR-206) in DIA.
(TIFF)

Figure S4 Expression levels of muscle-specific miRNAs in the serum of normal, carrier and dystrophy dogs ($CXMD_J$) at the indicated ages. Each Ct was determined by real-time PCR. In these graphs, the longer bars on each plot indicate the mean, and the shorter bars indicate ± SEM, n = 3. Asterisk (*) and pound (#) indicate a significant difference (*, $P<0.05$; **, $P<0.01$; ***, $P<0.001$ from normal: #, $P<0.05$; ##, $P<0.01$; ###, $P<0.001$ from carrier, one-way ANOVA with Bonferroni post hoc test). w: weeks; m: months.
(TIFF)

Acknowledgments

We would like to thank T. Yokota, M. Mori and K. Yuasa for critical feedback on the manuscript; M. Kobayashi, H. Kita, S. Ichikawa, Y. Yahata, T. Nakayama, K. Kinoshita, R. Nakagawa and Y. Kasahara (Department of Molecular Therapy) for assistance with the experiments.

Author Contributions

Conceived and designed the experiments: HM AN ST KH. Performed the experiments: HM YA NI SK. Analyzed the data: HM KH. Contributed reagents/materials/analysis tools: KY MS AN. Wrote the paper: HM.

References

1. Moser H (1984) Duchenne muscular dystrophy: pathogenetic aspects and genetic prevention. Hum Genet 66: 17–40.
2. Cullen MJ, Mastaglia FL (1980) Morphological changes in dystrophic muscle. Br Med Bull 36: 145–152.
3. Ervasti JM, Ohlendieck K, Kahl SD, Gaver MG, Campbell KP (1990) Deficiency of a glycoprotein component of the dystrophin complex in dystrophic muscle. Nature 345: 315–319.
4. Ebashi S, Toyokura Y, Momoi H, Sugita H (1959) High creatine phosphokinase activity of sera of progressive muscular dystrophy. J Biochem 46: 103–104.
5. Vassella F, Richterich R, Rossi E (1965) The Diagnostic Value of Serum Creatine Kinase in Neuromuscular and Muscular Disease. Pediatrics 35: 322–330.
6. Florence JM, Fox PT, Planer GJ, Brooke MH (1985) Activity, creatine kinase, and myoglobin in Duchenne muscular dystrophy: a clue to etiology? Neurology 35: 758–761.
7. Nicholson GA, Morgan GJ, Meerkin M, Strauss ER, McLeod JG (1986) The effect of aerobic exercise on serum creatine kinase activities. Muscle Nerve 9: 820–824.
8. Chen K, Rajewsky N (2007) The evolution of gene regulation by transcription factors and microRNAs. Nat Rev Genet 8: 93–103.
9. Ji X, Takahashi R, Hiura Y, Hirokawa G, Fukushima Y, et al. (2009) Plasma miR-208 as a Biomarker of Myocardial Injury. Clin Chem 55: 1944–1949.
10. Mitchell PS, Parkin RK, Kroh EM, Fritz BR, Wyman SK, et al. (2008) Circulating microRNAs as stable blood-based markers for cancer detection. Proc Natl Acad Sci USA 105: 10513–10518.
11. Wang K, Zhang S, Marzolf B, Troisch P, Brightman A, et al. (2009) Circulating microRNAs, potential biomarkers for drug-induced liver injury. Proc Natl Acad Sci USA 106: 4402–4407.
12. Valadi H, Ekström K, Bossios A, Sjöstrand M, Lee JJ, et al. (2007) Exosome-mediated transfer of mRNAs and microRNAs is a novel mechanism of genetic exchange between cells. Nat Cell Biol 9: 654–659.
13. Shimatsu Y, Katagiri K, Furuta T, Nakura M, Tanioka Y, et al. (2003) Canine X-linked muscular dystrophy in Japan (CXMDJ). Exp Anim 52: 93–97.
14. Urasawa N, Wada MR, Machida N, Yuasa K, Shimatsu Y, et al. (2008) Selective vacuolar degeneration in dystrophin-deficient canine Purkinje fibers despite preservation of dystrophin-associated proteins with overexpression of Dp71. Circulation 117: 2437–2448.
15. Yugeta N, Urasawa N, Fujii Y, Yoshimura M, Yuasa K, et al. (2006) Cardiac involvement in Beagle-based canine X-linked muscular dystrophy in Japan (CXMDJ): electrocardiographic, echocardiographic, and morphologic studies. BMC Cardiovasc Disord 6: 47.
16. Miska EA, Alvarez-Saavedra E, Townsend M, Yoshii A, Sestan N, et al. (2004) Microarray analysis of microRNA expression in the developing mammalian brain. Genome Biol 5: R68.
17. Chen J-F, Mandel EM, Thomson JM, Wu Q, Callis TE, et al. (2006) The role of microRNA-1 and microRNA-133 in skeletal muscle proliferation and differentiation. Nat Genet 38: 228–233.
18. Kim HK, Lee YS, Sivaprasad U, Malhotra A, Dutta A (2006) Muscle-specific microRNA miR-206 promotes muscle differentiation. J Cell Biol 174: 677–687.

19. McDaneld TG, Smith TPL, Doumit ME, Miles JR, Coutinho LL, et al. (2009) MicroRNA transcriptome profiles during swine skeletal muscle development. BMC Genomics 10: 77.
20. Yuasa K, Hagiwara Y, Ando M, Nakamura A, Takeda Si, et al. (2008) MicroRNA-206 is highly expressed in newly formed muscle fibers: implications regarding potential for muscle regeneration and maturation in muscular dystrophy. Cell Struct Funct 33: 163–169.
21. Shimatsu Y, Yoshimura M, Yuasa K, Urasawa N, Tomohiro M, et al. (2005) Major clinical and histopathological characteristics of canine X-linked muscular dystrophy in Japan, CXMDJ. Acta Myol 24: 145–154.
22. Greco S, De Simone M, Colussi C, Zaccagnini G, Fasanaro P, et al. (2009) Common micro-RNA signature in skeletal muscle damage and regeneration induced by Duchenne muscular dystrophy and acute ischemia. Faseb J 23: 3335–3346.
23. Williams AH, Valdez G, Moresi V, Qi X, McAnally J, et al. (2009) MicroRNA-206 delays ALS progression and promotes regeneration of neuromuscular synapses in mice. Science 326: 1549–1554.
24. Eisenberg I, Eran A, Nishino I, Moggio M, Lamperti C, et al. (2007) Distinctive patterns of microRNA expression in primary muscular disorders. Proc Natl Acad Sci U S A 104: 17016–17021.
25. Lodes MJ, Caraballo M, Suciu D, Munro S, Kumar A, et al. (2009) Detection of cancer with serum miRNAs on an oligonucleotide microarray. PLoS ONE 4: e6229.

HMG Advance Access published February 28, 2011

Human Molecular Genetics, 2011 **1–13**
doi:10.1093/hmg/ddr062

Matrix metalloproteinase-2 ablation in dystrophin-deficient *mdx* muscles reduces angiogenesis resulting in impaired growth of regenerated muscle fibers

Daigo Miyazaki[1], Akinori Nakamura[1,*], Kazuhiro Fukushima[1], Kunihiro Yoshida[1,2], Shin'ichi Takeda[3] and Shu-ichi Ikeda[1]

[1]Department of Medicine (Neurology and Rheumatology), Shinshu University School of Medicine, 3-1-1 Asahi, Matsumoto 390-8621, Japan, [2]Department of Neurogenetics, Division of Brain Disease Research, Shinshu University School of Medicine, 3-1-1 Asahi, Matsumoto 390-8621, Japan and [3]Department of Molecular Therapy, Institute of Neuroscience, National Research Center of Neurology and Psychiatry, 4-1-1 Ogawa-higashi, Kodaira, Tokyo 187-8521, Japan

Received October 12, 2010; Revised and Accepted February 8, 2011

Matrix metalloproteases (MMPs) are a family of endopeptidases classified into subgroups based on substrate preference in normal physiological processes such as embryonic development and tissue remodeling, as well as in various disease processes via degradation of extracellular matrix components. Among the MMPs, MMP-9 and MMP-2 have been reported to be up-regulated in skeletal muscles in the lethal X-linked muscle disorder Duchenne muscular dystrophy (DMD), which is caused by loss of dystrophin. A recent study showed that deletion of the *MMP9* gene in *mdx*, a mouse model for DMD, improved skeletal muscle pathology and function; however, the role of MMP-2 in the dystrophin-deficient muscle is not well known. In this study, we aimed at verifying the role of MMP-2 in the dystrophin-deficient muscle by using *mdx* mice with genetic ablation of MMP-2 (*mdx*/MMP-2$^{-/-}$). We found impairment of regenerated muscle fiber growth with reduction of angiogenesis in *mdx*/MMP-2$^{-/-}$ mice at 3 months of age. Expression of vascular endothelial growth factor-A (VEGF-A), an important angiogenesis-related factor, decreased in *mdx*/MMP-2$^{-/-}$ mice at 3 months of age. MMP-2 had not a critical role in the degradation of dystrophin–glycoprotein complex (DGC) components such as β-dystroglycan and β-sarcoglycan in the regeneration process of the dystrophic muscle. Accordingly, MMP-2 may be essential for growth of regenerated muscle fibers through VEGF-associated angiogenesis in the dystrophin-deficient skeletal muscle.

INTRODUCTION

Duchenne muscular dystrophy (DMD) is the most common severe X-linked muscular disorder, characterized by progressive muscle wasting and weakness (1). It is caused by a mutation in the *DMD* gene encoding the large cytoskeletal protein dystrophin (2). Dystrophin localizes to the sarcolemma of muscle fibers and forms a dystrophin–glycoprotein complex (DGC) with dystroglycans (DGs), sarcoglycans and syntrophin–dystrobrevin complexes, and DGC links the cytoskeletal protein actin to the basal lamina of muscle fibers (3). DGC may play a role in membrane stabilization during muscle contraction or act as a transducer of signals from the extracellular matrix (ECM) to the muscle cytoplasm via its interactions with intracellular signaling molecules (4). The loss of dystrophin leads to a condition in which the membrane is leaky under mechanical stress, and the subsequent increase in Ca^{2+} permeability results in activation of various proteases and alteration of the expression or function of dystrophin-associated plasma membrane proteins, such as neuronal nitric oxide synthase (nNOS), aquaporin-4 and ion channels (5). The pathology of the dystrophic muscle includes degeneration, necrosis with inflammatory cell invasion, regeneration and fibrous and fatty changes. However, the underlying

*To whom correspondence should be addressed. Tel: +81 263372673; Fax: +81 263373427; Email: anakamu@shinshu-u.ac.jp

mechanisms of ECM degradation, inflammation and fibrosis remain poorly understood.

ECM components have important roles in homeostasis and maintenance of muscle fiber functional integrity. Matrix metalloproteases (MMPs), a family of zinc-dependent endopeptidases, are key regulatory molecules in the formation, remodeling and degradation of ECM components in both physiological and pathological processes (6,7), such as tumor progression and metastasis, cerebrovascular and cardiovascular diseases and rheumatoid arthritis (8). Among the MMPs, MMP-2 (also called gelatinase A) and MMP-9 (also called gelatinase B) are involved in ECM remodeling of the skeletal muscle and in the dystrophic pathology of *mdx*, a mouse model for DMD (9). MMP-9 is produced by neutrophils and macrophages and is able to process β-DG, resulting in disruption of the link between the ECM and cell membrane in the dystrophin-deficient skeletal muscle from DMD patients (10–12). We previously reported that MMP-9 overexpresses in the *mdx* skeletal muscle after physical exercise (13) and may primarily be involved in the inflammatory process during muscle degeneration (14). Recently, it was reported that deletion of the *MMP9* gene in *mdx* mice reduces muscle inflammation and fibronecrosis, resulting in an improvement in muscle function (15). Based on these reports, MMP-9 may play an important role in ECM degradation in the dystrophin-deficient muscle.

MMP-2 is derived from vascular endothelial cells as well as smooth muscle cells and has a role in angiogenesis, based on observation of impaired angiogenesis in an ischemic model in MMP-2 knockout mice (16). We and other researchers have also demonstrated that MMP-2 may be associated with ECM remodeling during muscle regeneration and fiber growth (9,14). Moreover, MMP-2 may be involved in myogenesis (17) and muscle regeneration (18). However, the precise role of MMP-2 has not been fully elucidated in the dystrophic muscle. To better understand the role of MMP-2 in dystrophic pathology, we generated *mdx*/MMP-$2^{-/-}$ mice by crossing *mdx* with MMP-2 knockout mice (MMP-$2^{-/-}$) and examined the muscle pathology. Here, we demonstrate that MMP-2 ablation in *mdx* mice results in impairment of muscle fiber growth related to down-regulation of vascular endothelial growth factor-A (VEGF-A) when compared with *mdx*/MMP-$2^{+/+}$ mice. Moreover, expression of nNOS in 3-month-old *mdx*/MMP-$2^{-/-}$ mice was significantly lower than that in *mdx* mice. These results imply that MMP-2 may be required for growth of regenerated muscle fibers through angiogenesis by VEGF-A (hereafter, VEGF) in the dystrophin-deficient muscle.

RESULTS

MMP-2 ablation in *mdx* mice impairs growth of regenerated muscle fibers

To elucidate the role of MMP-2 in the dystrophin-deficient muscle, we crossed MMP-2 knockout (MMP-$2^{-/-}$) mice (19) with *mdx* mice with the genetic background of C57 BL/6J to generate *mdx*/MMP-$2^{-/-}$ mice. MMP-2 mRNA and its protein activity were absent in the skeletal muscle of both MMP-$2^{-/-}$ and *mdx*/MMP-$2^{-/-}$ mice, but not in wild-type (WT) and *mdx* mice (Supplementary Material, Fig. S1A and C). There was no statistically significant difference in the MMP-9 mRNA level in the skeletal muscle between the groups at 1 and 3 months of age (Supplementary Material, Fig. S1B). Although we could not detected MMP-9 protein activity on gelatin zymography in mice aged 3 months (Supplementary Material, Fig. S1C), the levels of both the pro- and active forms of MMP-9 protein levels were found to be significantly increased in *mdx* and *mdx*/MMP-$2^{-/-}$ mice when compared with the WT and MMP-$2^{-/-}$ mice at both 1 and 3 months of age (Supplementary Material, Fig. S1D–F). The discrepancy between the mRNA and protein levels of MMP-9 in the dystrophic skeletal muscle is speculated to be due to post-transcriptional regulation (20). MMP-3 mRNA levels were significantly elevated in the skeletal muscle of *mdx* and *mdx*/MMP-$2^{-/-}$ mice at 1 and 3 months of age when compared with that of the WT mice; the level was greatly increased in *mdx*/MMP-$2^{-/-}$ mice at 3 months of age (Supplementary Material, Fig. S1G). The mRNA levels of tissue inhibitor of metalloproteinase (TIMP)-1, an intrinsic inhibitor of MMP-9 and -3, were significantly up-regulated in the skeletal muscle of *mdx* and *mdx*/MMP-$2^{-/-}$ mice when compared with that of the WT mice at 1 and 3 months of age (Supplementary Material, Fig. S1H). There was no difference in the mRNA levels of TIMP-2, an intrinsic inhibitor of MMP-2, among the mouse groups at 1 or 3 months of age (Supplementary Material, Fig. S1I). In both MMP-$2^{-/-}$ mice (19) and *mdx*/MMP-$2^{-/-}$ mice, fertility and development were glossy normal. There were no differences in body weight at 1 or 3 months of age between *mdx* and *mdx*/MMP-$2^{-/-}$ or between WT and MMP-$2^{-/-}$ mice (Supplementary Material, Fig. S2A). Muscle power, evaluated using the hanging wire test and serum creatine kinase (CPK) levels, in *mdx*/MMP-$2^{-/-}$ at 3 months of age was not statistically different from that of *mdx* at the same age (Supplementary Material, Fig. S2B and C).

We then examined the histopathology of the skeletal muscle from *mdx*/MMP-$2^{-/-}$ mice. A previous study of *mdx* mice reported muscle necrosis with infiltration of neutrophils or macrophages at around 2 weeks of age, massive muscle degeneration/necrosis at around 1 month of age and completion of muscle necrosis with substitution of many regenerated fibers at 3 months of age (21). Histopathological findings for the tibialis anterior (TA) muscle from *mdx*/MMP-$2^{-/-}$ mice at 1, 2 and 3 months of age were roughly comparable to those of *mdx* mice at each age (Fig. 1A). However, we found that the muscle fibers, especially the centronuclear regenerated fibers, in *mdx*/MMP-$2^{-/-}$ mice at 3 months of age were significantly smaller than in *mdx* mice at the same age (Fig. 1B–E). Almost all of the small regenerated fibers in *mdx*/MMP-$2^{-/-}$ mice at 3 months of age were type II fibers, and a similar tendency was observed in *mdx* mice at the same age (Supplementary Material, Fig. S2D). We also analyzed diaphragm, quadriceps and gastrocnemius muscles in *mdx* and *mdx*/MMP-$2^{-/-}$ mice at 1 and 3 months of age. Like the TA muscle, these skeletal muscles in *mdx*/MMP-$2^{-/-}$ mice at 3 months of age exhibited impaired growth of regenerated fibers (Supplementary Material, Fig. S3). Furthermore, we monitored the muscle regeneration process as a result of cardiotoxin injury in the skeletal muscle of MMP-$2^{-/-}$ mice at 6 weeks of age. The result clearly

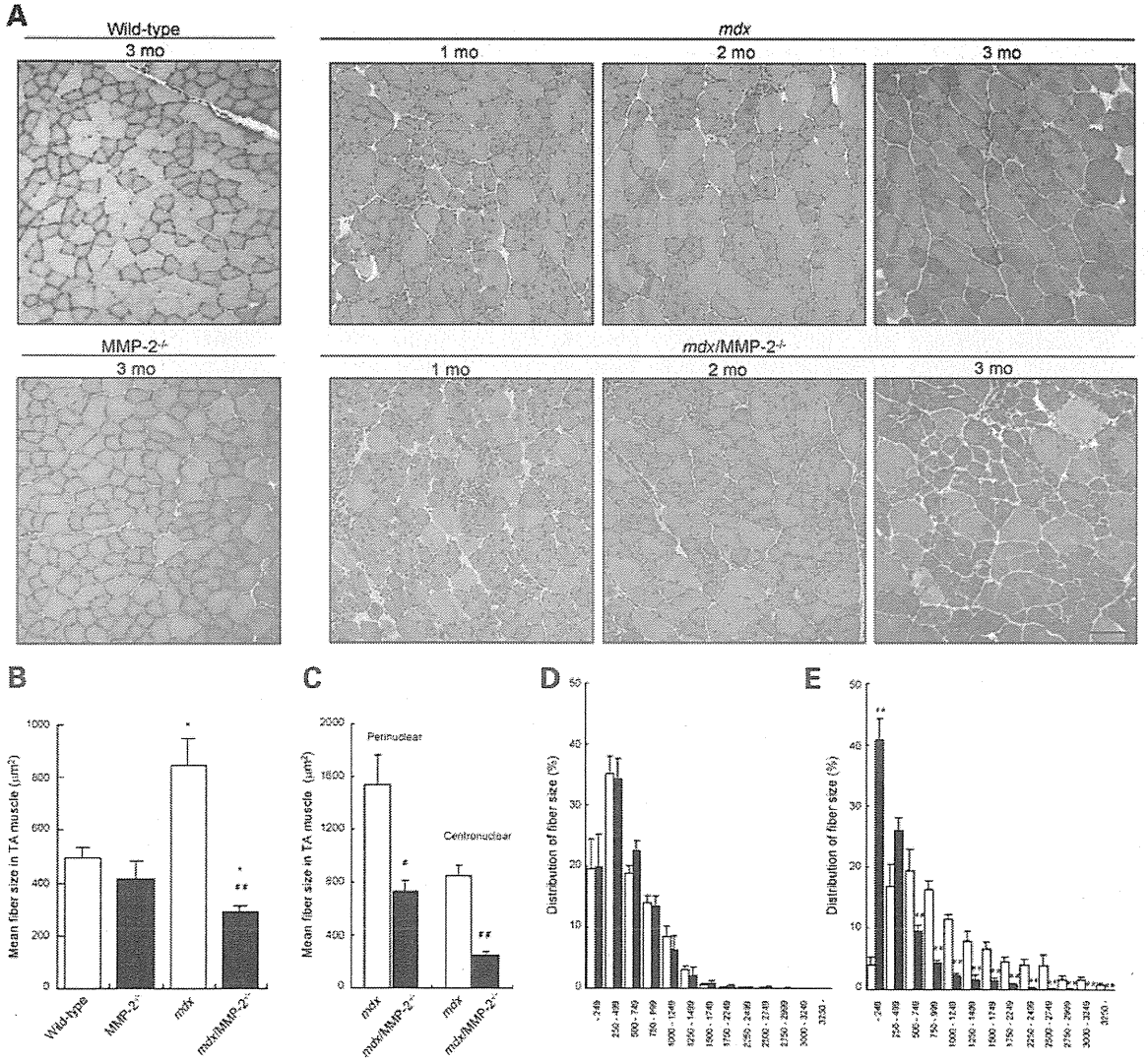

Figure 1. Histopathological characterization of the skeletal muscle of *mdx*/MMP-2$^{-/-}$ mice. (**A**) H&E staining of the TA muscles in *mdx* and *mdx*/MMP-2$^{-/-}$ mice at 1, 2 and 3 months of age. Scale bar: 100 μm. (**B**) The fiber size in the TA muscle at 3 months of age ($n = 3$ for each group). Bar: mean ± S.E.M.; $^{*}P < 0.05$, significantly different from WT; $^{\#\#}P < 0.01$, significantly different from MMP-2 ablation alone. (**C**) Comparison of perinuclear fibers and centronuclear regenerated fibers in the TA muscle at 3 months of age ($n = 3$ for each group). Bar: mean ± S.E.M.; $^{\#}P < 0.05$, $^{\#\#}P < 0.01$, significantly different from MMP-2 ablation alone. (**D**) Distribution of fiber size of the TA muscle in WT and MMP-2$^{-/-}$ mice at 3 months of age. Bar: mean ± S.E.M. (**E**) Distribution of fiber size of the TA muscle in *mdx* and *mdx*/MMP-2$^{-/-}$ mice at 3 months of age. Bar: mean ± S.E.M.; $^{\#\#}P < 0.01$, significantly different from MMP-2 ablation alone.

indicated that the centronuclear regenerating fibers 7 days after cardiotoxin injection in the skeletal muscle of MMP-2$^{-/-}$ mice were smaller than those of the WT (Supplementary Material, Fig. S4). These results suggest that ablation of MMP-2 may impair the growth of regenerated muscle fibers after the damage.

MMP-2 deficiency impairs angiogenesis in regenerated skeletal muscles of *mdx*

It has been reported that MMP-2 may be associated with angiogenesis, based on inhibition studies of MMP-2 (22,23). MMP-2 knockout mice have shown impairment of angiogenesis in an ischemia-induced model (16) and in a tumor model (24). To determine whether angiogenesis was impaired in the skeletal muscle of *mdx*/MMP-2$^{-/-}$ mice, we examined vessels in the TA muscle, through immunohistochemistry using an antibody to PECAM-1: an epithelial cell marker (Fig. 2A). We found that the mean size of vessels was significantly smaller in the skeletal muscle of *mdx*/MMP-2$^{-/-}$ mice at 3 months of age than that of age-matched *mdx* mice (Fig. 2B). Although the number of vessels per square millimeter was not different, the vessel counts per myofiber were significantly higher in *mdx* mice at 3 months of age, but decreased in age-matched *mdx*/MMP-2$^{-/-}$ mice (Fig. 2C and D). We also determined the endothelial area, which is

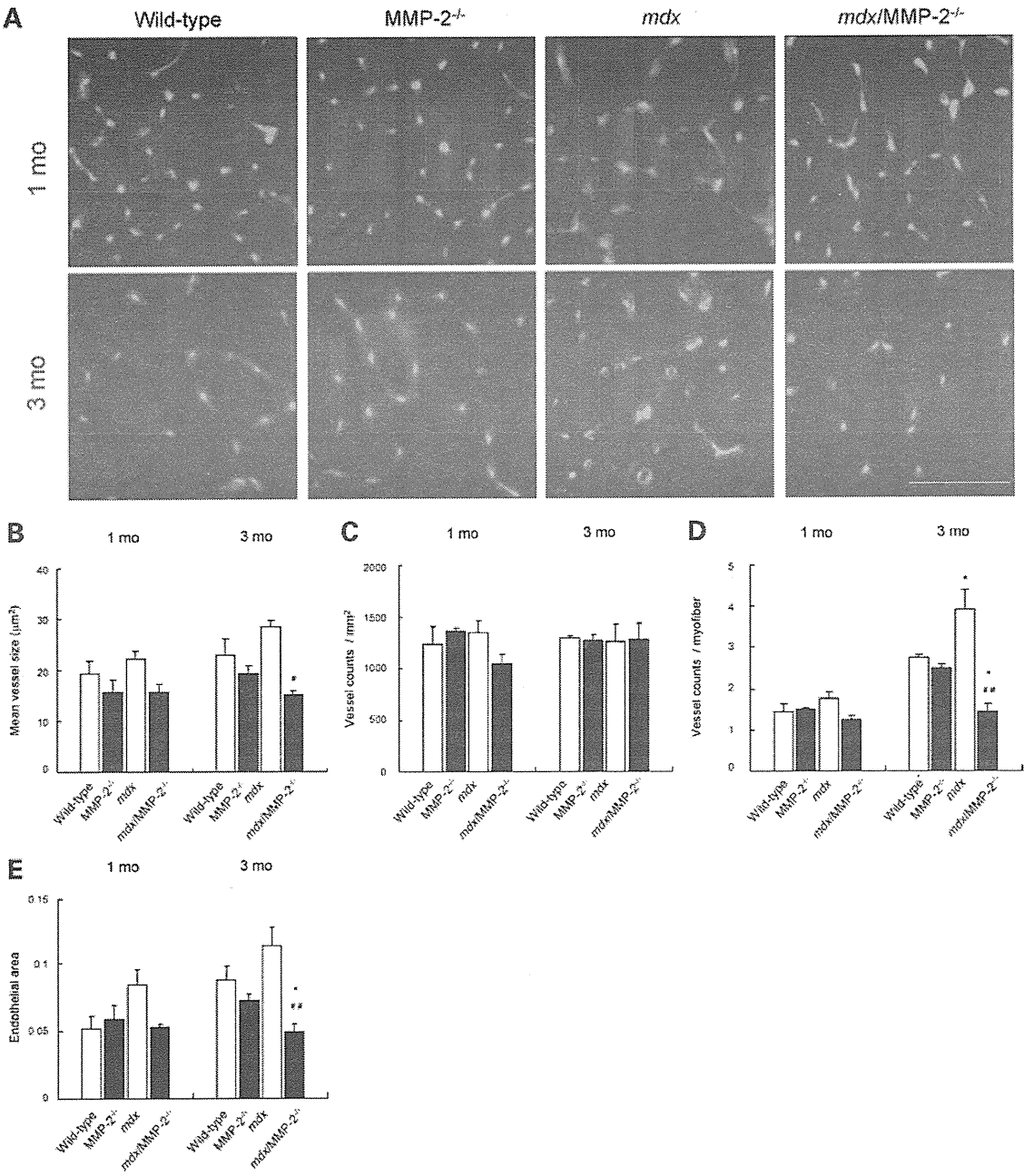

Figure 2. Evaluation of angiogenesis in the skeletal muscle of *mdx*/MMP-2$^{-/-}$ mice. (**A**) Immunohistochemistry with PECAM-1, an epithelial marker, in the TA muscle at 1 and 3 months of age. Scale bar: 100 μm. (**B**) Mean vessel size in the TA muscle of *mdx*/MMP-2$^{-/-}$ mice at 1 and 3 months of age ($n = 3$ for each group). Bar: mean ± S.E.M.; $^{\#}P < 0.05$, significantly different from MMP-2 ablation alone. (**C**) Number of vessels per square millimeter in the TA muscle at 1 and 3 months of age ($n = 3$ for each group). Bar: mean ± S.E.M. (**D**) Number of vessels per myofiber in the TA muscle at 1 and 3 months of age ($n = 3$ for each group). Bar: mean ± S.E.M.; $^{*}P < 0.05$, significantly different from WT; $^{\#\#}P < 0.01$, significantly different from MMP-2 ablation alone. (**E**) Endothelial area in the TA muscle of *mdx*/MMP-2$^{-/-}$ mice at 1 and 3 months of age ($n = 3$ for each group). Bar: mean ± S.E.M.; $^{*}P < 0.05$, significantly different from WT; $^{\#\#}P < 0.01$, significantly different from MMP-2 ablation alone.

equivalent to vascular bed, by multiplying the size of vessels by their number in the TA muscle. The endothelial area in *mdx*/MMP-2$^{-/-}$ mice at 3 months of age was significantly lower than that of the *mdx* mice at the same age (Fig. 2E). These results clearly indicate that MMP-2 ablation impairs angiogenesis in the *mdx* skeletal muscle.

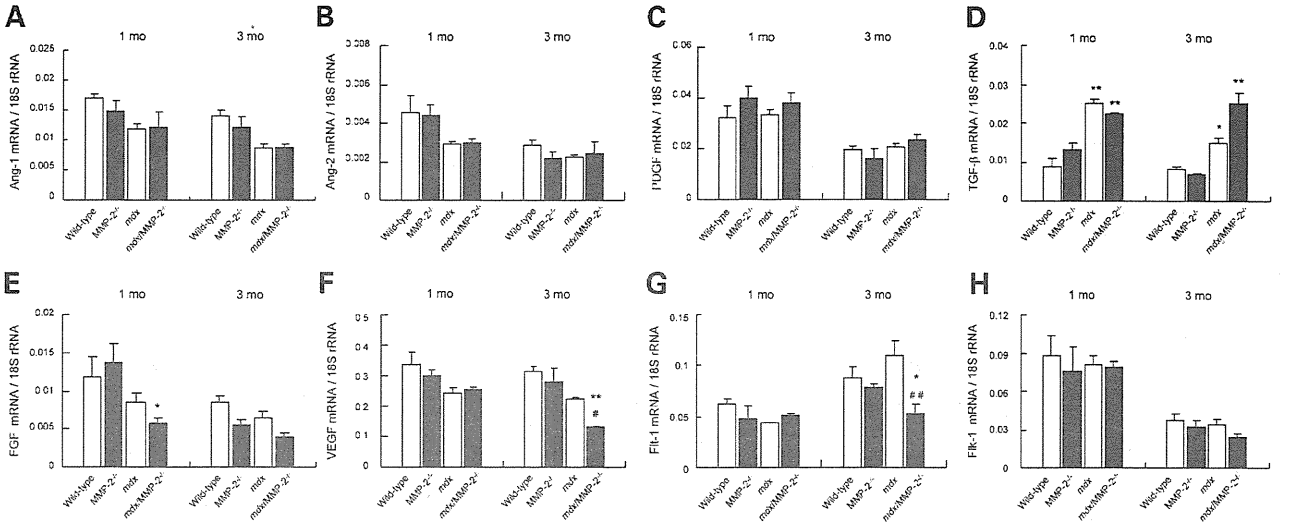

Figure 3. mRNA levels of various angiogenesis-related factors in the *mdx*/MMP-2$^{-/-}$ mice skeletal muscle. Relative (to 18S rRNA) mRNA levels of angiopoietin-1 (**A**), angiopoietin-2 (**B**), PDGF (**C**), FGF (**D**), TGF-β (**E**), VEGF (**F**) and VEGF receptor-1 (Flt-1) (**G**) and -2 (Flk-1) (**H**) in the skeletal muscle of WT, MMP-2$^{-/-}$, *mdx* and *mdx*/MMP-2$^{-/-}$ mice at 1 and 3 months of age ($n = 3$ for each group). Bar: mean ± S.E.M.; $^{*}P < 0.05$, $^{**}P < 0.01$, significantly different from WT; $^{\#}P < 0.05$, $^{\#\#}P < 0.01$, significantly different from MMP-2 ablation alone.

MMP-2 ablation in *mdx* mice down-regulates VEGF

We found that ablation of MMP-2 caused growth impairment of regenerated fibers and of angiogenesis in the *mdx* skeletal muscle at 3 months of age. We hypothesized that the growth impairment might be associated with the abnormality in angiogenesis; therefore, we examined the mRNA levels of various angiogenesis-related factors such as angiopoietin-1 and -2, platelet-derived growth factor (PDGF), fibroblast growth factor (FGF), transforming growth factor-β (TGF-β) and VEGF. No statistical differences in the levels of angiopoietin-1 or -2, PDGF or FGF were detected between *mdx* and *mdx*/MMP-2$^{-/-}$ mice or between WT and MMP-2$^{-/-}$ mice at 1 or 3 months of age (Fig. 3A–C and E). TGF-β mRNA levels were increased in *mdx* and *mdx*/MMP-2$^{-/-}$ mice when compared with WT, but did not significantly change with or without MMP-2 (Fig. 3D). However, we found a significant decrease in the VEGF mRNA level in *mdx*/MMP-2$^{-/-}$ mice when compared with *mdx* mice at 3 months of age (Fig. 3F). We also found a significant decrease in the mRNA level of Flt-1 (VEGF receptor 1), but not Flk-1 (VEGF receptor 2), in *mdx*/MMP-2$^{-/-}$ mice at 3 months of age (Fig. 3G and H). The VEGF protein level was significantly lower in the skeletal muscle of *mdx*/MMP-2$^{-/-}$ mice when compared with *mdx* mice at 3 months of age (Fig. 4A and B). VEGF was localized at neural cell adhesion molecule (NCAM)-positive muscle satellite cells and at the sarcolemma in some muscle fibers (Fig. 4C), but not at Mac-3-positive macrophages (Supplementary Material, Fig. S5). Flt-1 was also localized at most of the NCAM-positive muscle satellite cells. Flk-1-positive cells were identified as vascular endothelial cells by immunoreactivity of PECAM-1 (Fig. 4C). There were no differences in the localizations of VEGF, Flt-1 or Flk-1 between *mdx*/MMP-2$^{-/-}$ and *mdx* mice (Fig. 4C).

It has also been reported that MMP-2 is up-regulated in muscle regeneration in an experimentally injured model (9) and plays a role in myogenesis (17). To determine whether myogenic or growth factors are involved in pathogenesis in *mdx*/MMP-2$^{-/-}$ mice, we investigated the mRNA levels of the myogenic transcription factors Pax-3 and -7, MyoD, Myf5, myogenin and MEF2 in the skeletal muscle. However, there were no statistical differences in the levels of these factors between *mdx* and *mdx*/MMP-2$^{-/-}$ mice or between WT and MMP-2$^{-/-}$ mice at 1 or 3 months of age (Supplementary Material, Fig. S6A–F). There were also no differences in the mRNA levels of the growth factors such as insulin-like growth factor, myostatin or follistatin in the TA muscles between the two groups (Supplementary Material, Fig. S6G–I).

Overexpression of S100 proteins and cytokines in the skeletal muscle of *mdx*/MMP-2$^{-/-}$ mice at 3 months of age

As reported above, we examined the expression levels of various factors related to angiogenesis, myogenesis and growth in the skeletal muscle of *mdx*/MMP-2$^{-/-}$ mice. To determine whether other genes affect pathology in *mdx*/MMP-2$^{-/-}$ mice, we conducted microarrays to comprehensively identify differentially expressed genes in the skeletal muscle of *mdx* and *mdx*/MMP-2$^{-/-}$ mice at 1 and 3 months of age. Based on the profiles of all the genes, we found 113 genes that were differentially (>2- or <0.5-fold) affected by MMP-2 ablation (Supplementary Material, Table S1). Thirteen genes were up-regulated (Supplementary Material, Table S2) and 18 genes were down-regulated (Supplementary Material, Table S3) at 1 month of age, and 69 genes were up-regulated (Supplementary Material, Table S4) and 13 genes were down-regulated (Supplementary Material,

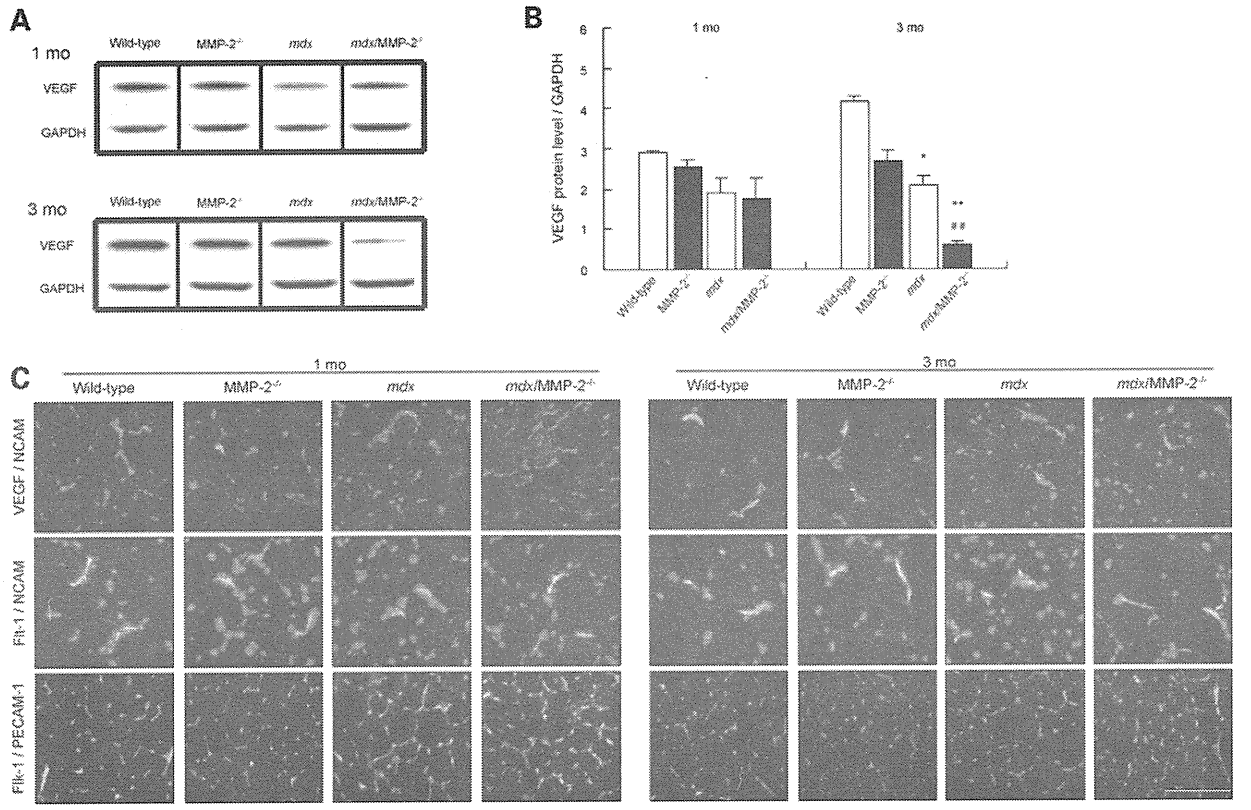

Figure 4. VEGF and its receptor protein levels and localization in the skeletal muscle of *mdx*/MMP-2$^{-/-}$. (**A**) Western blot analysis of VEGF (upper band) and internal control GAPDH (lower band) in WT, MMP-2$^{-/-}$, *mdx* and *mdx*/MMP-2$^{-/-}$ mice at 1 and 3 months of age. (**B**) Relative (to GAPDH) VEGF protein levels in WT, MMP-2$^{-/-}$, *mdx* and *mdx*/MMP-2$^{-/-}$ mice at 1 and 3 months of age ($n = 3$ for each group). Bar: mean ± S.E.M.; $^{*}P < 0.05$, $^{**}P < 0.01$, significantly different from WT; $^{\#\#}P < 0.01$, significantly different from MMP-2 ablation alone. (**C**) Immunohistochemistry of VEGF (red)/NCAM (green) (upper panel), Flt-1 (red)/NCAM (green) (middle panel) and Flk-1 (red)/PECAM-1 (green) (lower panel) in the skeletal muscle of WT, MMP-2$^{-/-}$, *mdx* and *mdx*/MMP-2$^{-/-}$ mice at 1 and 3 months of age. Scale bar: 100 μm.

Table S5) at 3 months of age in *mdx*/MMP-2$^{-/-}$ mice when compared with *mdx* mice (Supplementary Material, Fig. S7A and B). The genes that were up-regulated at 3 months of age in *mdx*/MMP-2$^{-/-}$ mice were mainly involved with protein binding, cytokine and its receptor or cell growth. Among the genes up-regulated at 3 months of age, S100 calcium-binding protein A8 (S100A8) and A9 (S100A9), cytokines such as chemokine C-C motif ligand (CCL)-2 and-7, chemokine C-C motif receptor (CCR)-1 and -2, and chitinase 3-like 3 were highly up-regulated in *mdx*/MMP-2$^{-/-}$ mice (Supplementary Material, Table S4). We confirmed these results by using quantitative real-time polymerase chain reaction (RT-PCR; Supplementary Material, Fig. S7C–I).

MMP-2 ablation further decreases nNOS expression in the skeletal muscle of *mdx* mice

Nitric oxide (NO) is a vasodilator produced by nitric oxide synthase (NOS), and inhibition of NOS activity abolishes capillary proliferation in electrically stimulated skeletal muscles (25). In electrically stimulated skeletal muscles, expression of endothelial NOS (eNOS) and nNOS increase in the early and late stages of angiogenesis, respectively (25–27). nNOS is linked to DGC, and dystrophin deficiency causes a reduction in nNOS expression at the sarcolemma, resulting in modification of dystrophic pathology (28,29). Thus, we examined the mRNA levels of nNOS, eNOS and inducible NOS (iNOS) produced by invaded inflammatory cells in the skeletal muscle of *mdx*/MMP-2$^{-/-}$ mice. mRNA expression of nNOS, but not of eNOS and iNOS, was significantly lower in *mdx*/MMP-2$^{-/-}$ than in *mdx* mice at 3 months of age (Fig. 5A–C). Western blotting also revealed that the nNOS protein level was significantly lower in *mdx*/MMP-2$^{-/-}$ than in *mdx* mice at 3 months of age (Fig. 5D and E), although there were no apparent differences in nNOS immunoreactivity between the *mdx*/MMP-2$^{-/-}$ and *mdx* mice (Fig. 5F). These results suggest that down-regulation of nNOS in the regenerated skeletal muscle of *mdx*/MMP-2$^{-/-}$ mice may influence impairment of angiogenesis.

MMP-2 does not affect the degradation of DGC components in the process of dystrophic muscle regeneration

DGs comprise two subunits, a highly glycosylated ECM protein, α-dystroglycan (α-DG), and a transmembrane

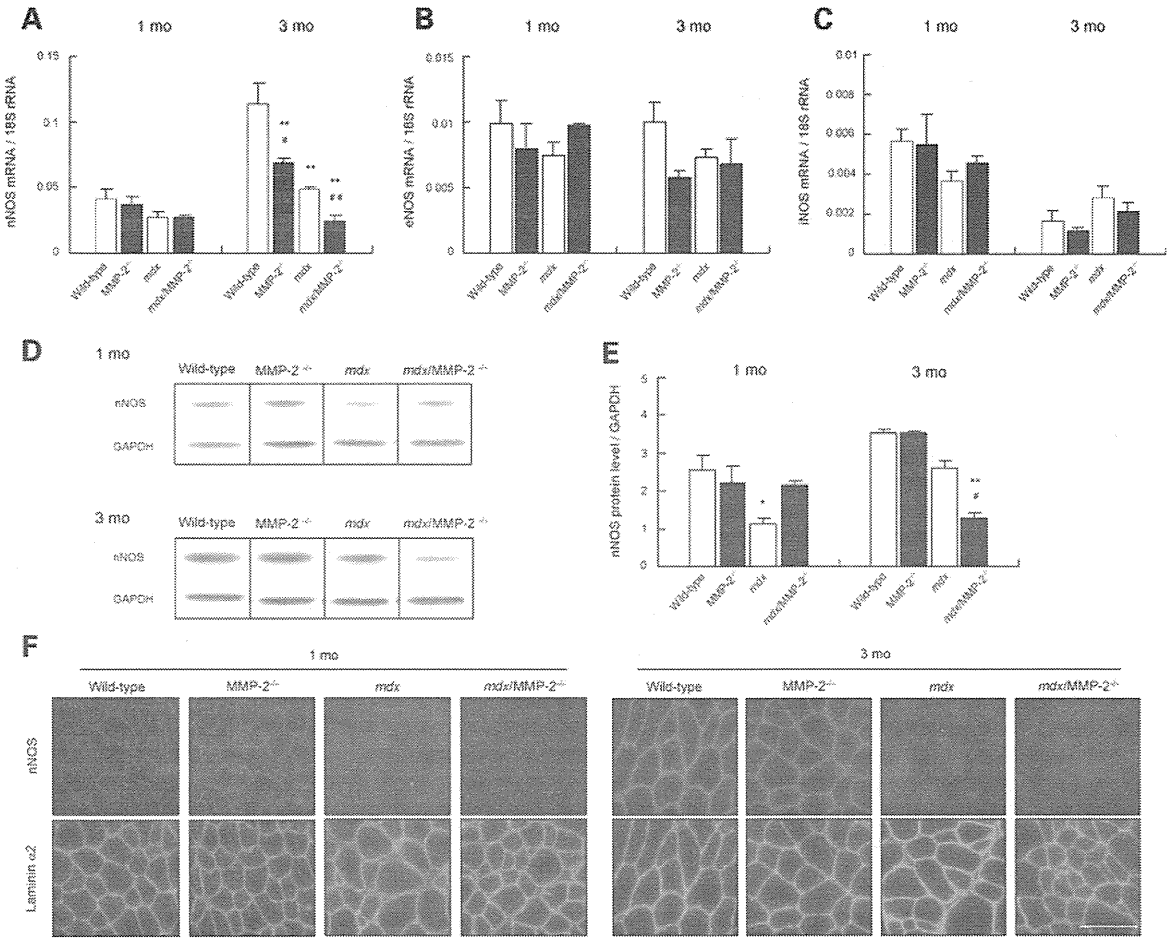

Figure 5. NOS isoform expression in the skeletal muscle of *mdx*/MMP-$2^{-/-}$ mice. Relative (to 18S rRNA) mRNA levels of nNOS (**A**), eNOS (**B**) and iNOS (**C**) in the skeletal muscle of WT, MMP-$2^{-/-}$, *mdx* and *mdx*/MMP-$2^{-/-}$ mice ($n = 3$ for each group). Bar: mean ± S.E.M.; $^{**}P < 0.01$, significantly different from WT; $^{\#}P < 0.05$, $^{\#\#}P < 0.01$, significantly different from MMP-2 ablation alone. (**D**) Western blot analysis of nNOS and (**E**) relative (to GAPDH) nNOS protein levels in the skeletal muscle of WT, MMP-$2^{-/-}$, *mdx* and *mdx*/MMP-$2^{-/-}$ mice ($n = 3$ for each group). Bar: mean ± S.E.M.; $^{*}P < 0.05$, $^{**}P < 0.01$, significantly different from WT; $^{\#}P < 0.05$, significantly different from MMP-2 ablation alone. (**F**) Immunohistochemistry of nNOS and laminin α2 in the skeletal muscle of WT, MMP-$2^{-/-}$, *mdx* and *mdx*/MMP-$2^{-/-}$ mice. Scale bar: 100 μm.

protein, β -dystroglycan (β-DG). DGs are membrane receptors involved with the complex of glycoproteins associated with dystrophin (30), and their interaction is crucial in maintaining the integrity of the plasma membrane. In the dystrophin-deficient muscle, the interaction between the two DG subunits may be disrupted by the proteolytic activity of MMPs (12). Previous research has examined the proteolytic activities of human MMP-9 and MMP-2 on the recombinant extracellular domain of β-DG and characterized a cleavage site by MMP-9 on β-DG (31). However, the molecular mechanism underlying the effect of MMP-2 is still unknown. We examined whether MMP-2 ablation in *mdx* mice affects processing of DGC in the skeletal muscle. In the skeletal muscle of both *mdx* and *mdx*/MMP-$2^{-/-}$ mice at 1 and 3 months of age, full-length 43-kDa β-DG (βDG_{43}) was cleaved to a 30-kDa form of β-DG (βDG_{30}) (Fig. 6A); however, although the degree of degradation in *mdx*/MMP-$2^{-/-}$ mice was less than that in *mdx* mice at 1 month of age, it was not different at 3 months of age (Fig. 6B and C). Similarly, expression of β-sarcoglycan did not change in the skeletal muscle of *mdx*/MMP-$2^{-/-}$ mice at 1 or 3 months of age when compared with *mdx* of the same age (Supplementary Material, Fig. S8). In the process of regeneration of the dystrophic muscle, MMP-2 may not have a critical role in the degradation of DGC components.

DISCUSSION

In this study, we investigated the role of MMP-2 in the dystrophic skeletal muscle using *mdx* mice with MMP-2 ablation (*mdx*/MMP-$2^{-/-}$). The histopathology of the skeletal muscle in *mdx*/MMP-$2^{-/-}$ mice at 3 months of age showed small regenerated muscle fibers and an impairment of angiogenesis when compared with *mdx* mice at the same age. The impaired growth of regenerating muscle fibers was also observed in the

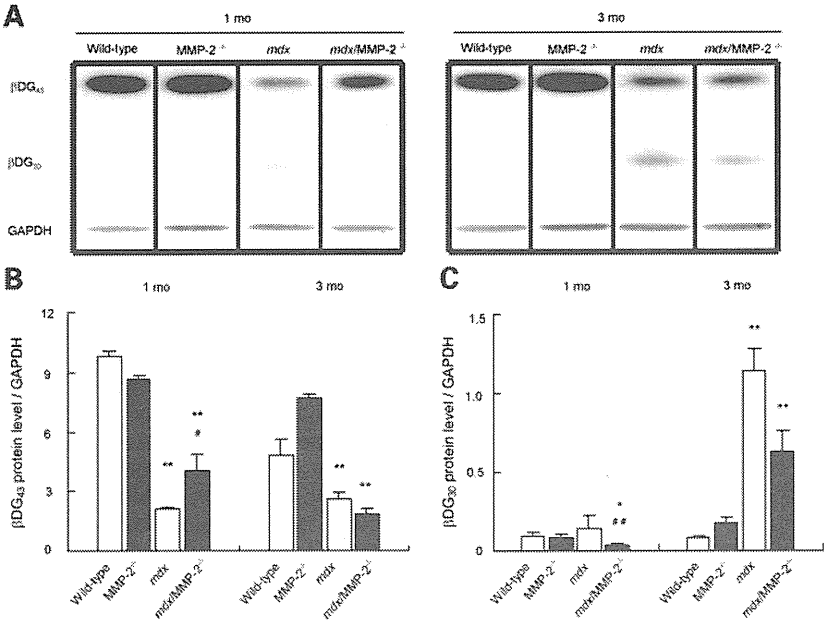

Figure 6. β-DG degradation in the *mdx*/MMP-2$^{-/-}$ mice skeletal muscle. (**A**) Western blot analyses of β-DG in the skeletal muscle of WT, MMP-2$^{-/-}$, *mdx* and *mdx*/MMP-2$^{-/-}$ mice. Full-length β-DG (βDG_{43}, upper bands) and degraded 30-kDa proteins (βDG_{30}, lower bands) were observed in both *mdx* or *mdx*/MMP-2$^{-/-}$ mice at 1 and 3 months of age. Relative (to GAPDH) levels of βDG_{43} (**B**) and βDG_{30} (**C**) revealed an increase in βDG_{43} and a decrease in βDG_{30} in *mdx*/MMP-2$^{-/-}$ when compared with *mdx* at 1 month of age. Bar: mean ± S.E.M.; $^{*}P < 0.05$, $^{**}P < 0.01$, significantly different from WT; $^{\#}P < 0.05$, $^{\#\#}P < 0.01$, significantly different from MMP-2 ablation alone.

cardiotoxin injury model of MMP-2$^{-/-}$ mice, suggesting that MMP-2 may play an important role in the muscle regeneration under certain disease conditions. MMP-2, a primary MMP derived from vascular endothelial cells and smooth muscle cells, degrades various ECM proteins (32,33) and is implicated as a key player in vascular development and angiogenesis (34). MMP-2 knockout mice have demonstrated a reduction in angiogenesis and corresponding tumor growth (24) and impairment of ischemia-induced neovascularization through a decreased number of endothelial cells and endothelial progenitor cells (16). Therefore, we hypothesized that the close relationship between impairment of regenerated myofiber growth and reduction in angiogenesis in the *mdx*/MMP-2$^{-/-}$ mice might allow us to identify factors related to angiogenesis or growth in these mice. We subsequently found a reduction of VEGF expression in the regenerated skeletal muscle of the mice at 3 months of age.

VEGF plays an important role in mediating both physiological and pathological angiogenesis via inducing vasodilation or vascular permeability, and by stimulating the proliferation, migration and survival of endothelial cells (35). In a previous study, both cultured satellite cells and myoblasts expressed VEGF and VEGFR-1 and -2; furthermore, administration *in vitro* stimulates myoblast migration and survival, protects myogenic cells from apoptosis and promotes myogenic cell growth (36). In normal muscles, VEGF and its receptors are expressed in vascular structures and not in muscle fibers; however, they are expressed in satellite cells and regenerating muscle fibers after experimental muscle damage, suggesting the operation of an autocrine pathway that may promote the survival and regeneration of myocytes (37). This study also demonstrates that the introduction of VEGF by using a virus vector promotes regeneration via angiogenesis, resulting in the decrease in muscle damage as well as the promotion of muscle regeneration and function in *mdx* mice (37). Meanwhile, another study shows that VEGF administration by using viral vectors injected in the normal mouse skeletal muscle results in the appearance of a notable subset of muscle fibers exhibiting muscle regeneration. Moreover, the delivery of VEGF markedly promotes muscle fiber regeneration with a dose-dependent effect after experimental muscle damage with ischemia, glycerol or cardiotoxin (38). Furthermore, the increased density of satellite cells has been observed adjacent to capillaries, suggesting a possible role of VEGF in homing circulating progenitor germ cells to specific muscle location and/or in regulating the satellite cells pool (39). Taken together, VEGF might function during regeneration not only through neovascularization, but also by directly acting on muscle cells and on the recruitment of progenitor cells from bone marrow during dystrophic pathology. VEGF was down-regulated in an ischemic-induced model using MMP-2 knockout mice due to a reduction in the number of invasive macrophages producing VEGF (16). However, our data indicate that VEGF is localized in NCAM-positive satellite cells and the sarcolemma in certain muscle fibers (Fig. 4C), but not in Mac-3-positive macrophages (Supplementary Material, Fig. S5). In a recent report, MMP-2 transcriptional inactivation by using an siRNA-based approach both in *in vitro* and *in vivo* significantly reduced integrin-αVβ3-mediated phosphoinositide 3-kinase/AKT-induced VEGF expression, which ultimately decreased tumor cell-induced angiogenesis (40). Similar mechanism might also underlie the relationship between MMP-2 and VEGF in the